Symplectic Hamiltonian finite element methods for linear elastodynamics

Manuel A. Sánchez[1]

Institute for Mathematical and Computational Engineering, School of Engineering and Faculty of Mathematics, Pontificia Universidad Católica de Chile, Santiago, Chile

Bernardo Cockburn[2]

School of mathematics, University of Minnesota, Minneapolis, MN 55455, USA

Ngoc-Cuong Nguyen[3]

Department of Aeronautics and Astronautics, Massachusetts Institute of Technology, Cambridge, MA 02139, USA

Jaime Peraire[3]

Department of Aeronautics and Astronautics, Massachusetts Institute of Technology, Cambridge, MA 02139, USA

Abstract

We present a class of high-order finite element methods that can conserve the linear and angular momenta as well as the energy for the equations of linear elastodynamics. These methods are devised by exploiting and preserving the Hamiltonian structure of the equations of linear elastodynamics. We show that several mixed finite element, discontinuous Galerkin, and hybridizable discontinuous Galerkin (HDG) methods belong to this class. We discretize the semidiscrete Hamiltonian system in time by using a symplectic integrator in order to ensure the symplectic properties of the resulting methods, which are called symplectic Hamiltonian finite element methods. For a particular semidiscrete HDG method, we obtain optimal error estimates and present, for the symplectic Hamiltonian HDG method, numerical experiments that confirm its optimal orders of convergence for all variables as well as its conservation properties.

Keywords:

Email addresses: `manuel.sanchez@uc.cl` (Manuel A. Sánchez), `cockburn@math.umn.edu` (Bernardo Cockburn), `cuongng@mit.edu` (Ngoc-Cuong Nguyen), `peraire@mit.edu` (Jaime Peraire)

[1]M. A. Sánchez was partially supported by FONDECYT Iniciación n.11180284 grant

[2]B. Cockburn was partially supported by NSF via DMS-1912646 grant.

[3]N.-C. Nguyen and J. Peraire were partially supported by NASA (under grant number NNX16AP15A) and the AFOSR (under grant number FA9550-16-1-0214).

Elastodynamics, symplectic Hamiltonian finite element methods, mixed methods, discontinuous Galerkin methods, hybridizable discontinuous Galerkin methods
2010 MSC: 65M60, 74H15, 74J05, 74S05

1. Introduction

Elastodynamics is a Hamiltonian system endowed with crucial properties such as symplectic structure and Hamiltonian preservation. In addition, in the absence of external loading and dissipation, elastodynamics exhibits fundamental conservation properties in linear momentum and angular momentum as well as the total energy. These fundamental properties of elastodynanmics play a key role both in mathematics and engineering applications. Numerical discretizations of elastodynamics need not, and in general will not, inherit the Hamiltonian structure as well as the conservation of both momentum and energy. Discretization schemes that do not conserve momentum and energy often suffer from error accumulation for long time-integration. Therefore, it is of considerable interest to develop numerical methods that inherit these crucial properties of elastodynamics. Significant attention has been paid to the development of time-integration schemes that conserve momentum and energy for elastodynamics [16, 18, 17, 24, 37, 37, 39, 38]. In order for the fully discrete system resulting from temporal and spatial discretizations of elastodynamics to inherit its Hamiltonian structure, the spatial discretization method must result in a Hamiltonian semidiscrete system and the time-integration scheme must be symplectic. When such space discretization is a finite element method, we call the resulting numerical method a symplectic Hamiltonian finite element method.

Pioneering works on numerical methods based on finite element discretizations which took advantage of the Hamiltonian structure of the equations of elastodynamics are the 2001 method in [6] and the 2005 method proposed in [21]. Although the time-marching method proposed in [6] was dissipative and only second-order accurate, the time-marching method proposed in [21] was exactly non-dissipative and could achieve high-order accuracy of any order. The authors managed to prove, through remarkable manipulations, that their time-marching method defines a Hamiltonian system which conserves the discrete Hamiltonian. On the other hand, it is interesting to note that the time-marching method is equivalent to a Runge-Kutta Gauss method and is symplectic. So, in hindsight, it is not a surprise that the resulting method defines a Hamiltonian dynamical system. The method proposed in [21] seems to be, to the best of our knowledge, the first symplectic Hamiltonian finite element method.

The second symplectic Hamiltonian finite element method was proposed in 2008, [42]. It used the discontinuous Galerkin (DG) method for the space discretization of some linear hyperbolic systems like the rotating shallow water equations, and the acoustic wave and 2D Maxwell equations. The resulting DG method coincided with the classic DG method with alternating fluxes devised back in 2002 in [43] in the case in which the material parameters are constant.

However, a crucial difference is that in the method proposed in [42], the discretization in time is carried out by means of a symplectic method in order to prevent the drifting of the energy. In 2013, this approach was applied to the linearized incompressible Euler equations [33]. In 2015, a third symplectic Hamiltonian finite element method was proposed in [23]. The discretization by the mixed method was proven to preserve the Hamiltonian structure of the acoustic wave equation. The resulting semidiscrete scheme was then discretized in time with symplectic methods [23]. Also in 2015, a new DG method was introduced by using the Lagrangian structure of the acoustic wave equation in [3]; no mention of symplectic time-marching schemes was made though. In 2018, a similar construction was carried out for the equations of elastodynamics in [4].

In 2017, we proposed the first symplectic Hamiltonian finite element method using the HDG method to discretize in space the acoustic wave equation [36]. In this paper, we extend that work and show how to devise symplectic Hamiltonian finite element methods for the equations of elastodynamics on a domain Ω in $\mathbb{R}^d$, $d = 2, 3$, namely,

$$\rho\,\ddot{\boldsymbol{u}} - \nabla\cdot(\mathcal{C}\,\underline{\boldsymbol{\epsilon}}(\boldsymbol{u})) = \boldsymbol{f}, \quad \text{in } \Omega,\ \forall t \in (0, T], \tag{1a}$$

with boundary and initial conditions

$$\boldsymbol{u} = \boldsymbol{u}_D \quad \text{on } \Gamma_D \times (0, T], \quad \mathcal{C}\,\underline{\boldsymbol{\epsilon}}(\boldsymbol{u})\boldsymbol{n} = \boldsymbol{\sigma}_N \quad \text{on } \Gamma_N \times (0, T], \tag{1b}$$

$$\boldsymbol{u}(0) = \boldsymbol{u}_0, \quad \dot{\boldsymbol{u}}(0) = \boldsymbol{v}_0 \quad \text{in } \Omega. \tag{1c}$$

For simplicity, we discretize the above equations in space by using mixed (using the compliance tensor), DG and HDG (using the stiffness tensor) methods. The DG and HDG methods, can be viewed as stabilized mixed methods, [11], like the mixed methods constructed by the Hu-Washizu variational principle, see, for example, [5, 9, 25].

We show that, as a direct consequence of the Hamiltonian structure of these methods, <u>the linear and angular momenta, and the total energy remain constant in time whenever $\Gamma_D = \emptyset$, and $\boldsymbol{f}$ and $\boldsymbol{\sigma}_N$ are zero.</u>

In the equation of motion (1a), the vector displacement is denoted by $\boldsymbol{u}$, the linearized strain tensor is denoted by $\underline{\boldsymbol{\epsilon}}(\boldsymbol{u}) := (\nabla\boldsymbol{u} + \nabla\boldsymbol{u}^{\mathrm{T}})/2$, and the divergence operator acting on tensor-valued functions is denoted by $\nabla\cdot$. We assume that Ω is a bounded polygonal domain in $\mathbb{R}^d$ with Lipschitz boundary $\partial\Omega =: \Gamma_D \cup \Gamma_N$ and $\Gamma_D \cap \Gamma_N = \emptyset$, the density $\rho = \rho(\boldsymbol{x})$ is a positive and bounded function, the stiffness tensor $\mathcal{C} = \mathcal{C}(\boldsymbol{x})$ is a symmetric, positive definite as bounded linear operator, and the data $\boldsymbol{f}(t)$, $\boldsymbol{u}_D(t)$ and $\boldsymbol{\sigma}_N(t)$ lie in $[L^2(\Omega)]^d$, $H^{1/2}(\Gamma_D)^d$ and $H^{-1/2}(\Gamma_N)^d$, respectively, for all $t \geq 0$. We omit the space dependence of the variables and only display their time dependence. We use the dot (Newton's) notation for the time derivatives and the standard notation of differential operators for spatial differentiation [36].

This paper can be considered as a stepping stone toward devising symplectic Hamiltonian finite element methods for the equations of large deformation.

Here, our goal is to devise methods for linear elastodynamics which conserve the linear and angular momenta as well as the energy. We have three main contributions. The first is that we show how to achieve this not only for the HDG method but for a wide variety of finite element discretizations. The second is that we switch from the canonical Hamiltonian formulation used in [36] to the formulation using Poisson brackets and prove that they are equivalent. The third is that we obtain optimal error estimates for all the approximate variables of the HDG method. Therefore, the approximate stress and strain of the HDG method converges one order higher than those of traditional finite element methods such as DG methods [42] and continuous Galerkin (CG) methods.

Our approach is different from the one used in [42, 33] because we do not obtain the space discretization by constructing a a suitable discrete Poisson bracket which would guarantee the Hamiltonian structure of the resulting discretization. Instead, we directly verify that several schemes, mixed, HDG and DG, do have such a structure. A similar difference can be made between our work and that in [3, 4] since they use the Lagrangian formulation of the equations instead of the Hamiltonian one, and since they do not advocate the use of symplectic time-integrators. Finally, let us point out that our approach is closest to the one carried out in [23] but we do use a different Hamiltonian, and we show how to handle the case in which the Neumann condition is different from zero.

The organization of the paper is as follows. In the next section, we give the modern definition of a Hamiltonian dynamical system and we show that the equations of elastodynamics define one. We also show the three conservation laws we are interested in by using the Hamiltonian structure of the equations. In Section 3, we display examples of Hamiltonian finite element methods. In Section 4, we prove that these spatial discretizations yield semidiscrete schemes with a Hamiltonian structure. We also show that, as a consequence, the three conservation laws under consideration also hold. In Section 5, we obtain the symplectic Hamiltonian finite element method by discretizing in time with a symplectic method. In Section 6, we carry out several numerical experiments which confirm the high-order accuracy and the conservation properties of the so-called HDG$_k$+ method. We end briefly discussing some extensions and ongoing work.

2. The Hamiltonian structure of elastodynamics

In this section, we describe the main properties of the exact solution which we want to preserve under discretization. We start by showing that, when the data $\boldsymbol{f}$, $\boldsymbol{\sigma}_N$ and $\boldsymbol{u}_D$ are independent of time, the equations of elastodynamics define a Hamiltonian dynamical system. We then use this information to deduce the conservation laws of linear elastodynamics, namely, those of the linear and angular momenta, and that of the energy.

2.1. A Hamiltonian formulation

We rewrite the boundary-value problem for the equation of elastodynamics as a first-order system as follows:

$$\begin{aligned} \dot{\boldsymbol{u}} &= \boldsymbol{v} && \text{in } \Omega \times (0,T], && \text{(2a)}\\ \rho\,\dot{\boldsymbol{v}} &= \nabla\cdot(\mathcal{C}\underline{\boldsymbol{\epsilon}}(\boldsymbol{u})) + \boldsymbol{f} && \text{in } \Omega \times (0,T], && \text{(2b)}\\ \boldsymbol{u} &= \boldsymbol{u}_D && \text{on } \Gamma_D \times (0,T], && \text{(2c)}\\ \mathcal{C}\underline{\boldsymbol{\epsilon}}(\boldsymbol{u})\boldsymbol{n} &= \boldsymbol{\sigma}_N && \text{on } \Gamma_N \times (0,T]. && \text{(2d)} \end{aligned}$$

If we consider that the mappings $t \mapsto (\boldsymbol{u}(t), \boldsymbol{v}(t))$ are orbits on a smooth manifold $\mathcal{M}$, the above boundary-value problem can be considered as a dynamical system. We want to show that this is a Hamiltonian dynamical system.

To define such a system, we use a slight extension of the definition of a Hamiltonian system used in [30], see also [29]. We say that the above system is a Hamiltonian dynamical system (or that it has a Hamiltonian formulation or that it has a Hamiltonian structure) if we can rewrite it as

$$\dot{C} = \{C, H\}, \tag{3}$$

for the coordinates functionals C, defined on the phase affine space $\mathcal{M}$, which are identified with a space of test functions $\mathcal{T}$. Here H is the Hamiltonian, a functional on $\mathcal{M}$; $\{\cdot,\cdot\}$ is the Poisson bracket, a bilinear form on the space of linear functionals on $\mathcal{M}$ which satisfies the so-called Jacobi identity.

In [30], the triple $(\mathcal{M}, \{\cdot,\cdot\}, H)$ is called a Hamiltonian dynamical system. With our definition, we also have to specify the coordinates functionals C and the space of test functions $\mathcal{T}$. This is the only, slight difference between the original definition of a Hamiltonian dynamical system in [30] and the one used here. We find this addition useful when dealing with weak formulations of the equations and with those of their discretizations.

Let us show that the equations of elastodynamics define a Hamiltonian dynamical system. We first consider the case in which the data $\boldsymbol{f}$, $\boldsymbol{\sigma}_N$ and $\boldsymbol{u}_D$ are independent of time. In this case, the Hamiltonian is

$$\begin{aligned} H(\boldsymbol{u}(t), \boldsymbol{v}(t)) = &\frac{1}{2}\int_\Omega (\rho\,\boldsymbol{v}(t)\cdot\boldsymbol{v}(t) + \mathcal{C}\underline{\boldsymbol{\epsilon}}(\boldsymbol{u}(t)) : \underline{\boldsymbol{\epsilon}}(\boldsymbol{u}(t))) \\ &- \int_\Omega \boldsymbol{f}\cdot\boldsymbol{u}(t) - \int_{\Gamma_N} \boldsymbol{\sigma}_N\cdot\boldsymbol{u}(t) \end{aligned} \tag{4a}$$

Note that the Hamiltonian coincides with the energy only when $\boldsymbol{f}$ and $\boldsymbol{\sigma}_N$ are zero. The Poisson bracket is

$$\{F, G\} = \int_\Omega \rho^{-1}\left(\frac{\delta F}{\delta \boldsymbol{u}}\cdot\frac{\delta G}{\delta \boldsymbol{v}} - \frac{\delta F}{\delta \boldsymbol{v}}\cdot\frac{\delta G}{\delta \boldsymbol{u}}\right), \tag{4b}$$

for $F = F(\boldsymbol{u}, \boldsymbol{v})$ and $G = G(\boldsymbol{u}, \boldsymbol{v})$ functionals on $\mathcal{M}$, where $\frac{\delta F}{\delta \boldsymbol{u}}$ and $\frac{\delta F}{\delta \boldsymbol{v}}$ denote the functional derivatives of the functional F. We then have that

$$\begin{aligned}\delta H &= \lim_{\varepsilon\to 0}\frac{1}{\varepsilon}\Big(H(\boldsymbol{v}+\varepsilon\delta\boldsymbol{v},\boldsymbol{u}+\varepsilon\delta\boldsymbol{u})-H(\boldsymbol{v},\boldsymbol{u})\Big)\\ &= \int_\Omega (\rho\,\boldsymbol{v}\cdot\delta\boldsymbol{v}+\mathcal{C}\underline{\boldsymbol{\epsilon}}(\boldsymbol{u}):\underline{\boldsymbol{\epsilon}}(\delta\boldsymbol{u}))-\int_\Omega \boldsymbol{f}\cdot\delta\boldsymbol{u}-\int_{\Gamma_N}\boldsymbol{\sigma}_N\cdot\delta\boldsymbol{u},\end{aligned}$$

that the phase manifold and the space of test functions are given by

$$\mathcal{M}=\{\boldsymbol{\omega}\in L^2(\Omega)^d:\ \nabla\cdot(\mathcal{C}\underline{\boldsymbol{\epsilon}}(\boldsymbol{\omega}))\in L^2(\Omega)^d,\ \boldsymbol{\omega}=\boldsymbol{u}_D \text{ on } \Gamma_D\}\times L^2(\Omega)^d, \tag{4c}$$

$$\mathcal{T}=\mathcal{C}^\infty(\Omega)^d\times\{\boldsymbol{\eta}\in\mathcal{C}^\infty(\Omega)^d:\ \boldsymbol{\eta}=\boldsymbol{0}\text{ on }\Gamma_D\}, \tag{4d}$$

and the coordinates functionals are

$$C_{\boldsymbol{u}}(\boldsymbol{\phi})=\int_\Omega \rho\,\boldsymbol{u}\cdot\boldsymbol{\phi},\quad C_{\boldsymbol{v}}(\boldsymbol{\psi})=\int_\Omega \rho\,\boldsymbol{v}\cdot\boldsymbol{\psi}, \tag{4e}$$

for $(\boldsymbol{\phi},\boldsymbol{\psi})\in\mathcal{T}$. Now, by taking $C := C_{\boldsymbol{u}}(\boldsymbol{\phi})$ and $C := C_{\boldsymbol{v}}(\boldsymbol{\psi})$ in the equation (3), we obtain

$$\int_\Omega \rho\,\dot{\boldsymbol{u}}\cdot\boldsymbol{\phi}=\dot{C}_{\boldsymbol{u}}(\boldsymbol{\phi})=\{C_{\boldsymbol{u}}(\boldsymbol{\phi}),H\}=\int_\Omega \rho^{-1}\frac{\delta C_{\boldsymbol{u}}(\boldsymbol{\phi})}{\delta\boldsymbol{u}}\cdot\frac{\delta H}{\delta\boldsymbol{v}}=\int_\Omega \rho\,\boldsymbol{v}\cdot\boldsymbol{\phi}, \tag{5a}$$

$$\int_\Omega \rho\,\dot{\boldsymbol{v}}\cdot\boldsymbol{\psi}=\dot{C}_{\boldsymbol{v}}(\boldsymbol{\psi})=\{C_{\boldsymbol{v}}(\boldsymbol{\psi}),H\}=-\int_\Omega \rho^{-1}\frac{\delta C_{\boldsymbol{v}}(\boldsymbol{\psi})}{\delta\boldsymbol{v}}\cdot\frac{\delta H}{\delta\boldsymbol{u}} \tag{5b}$$

$$=-\int_\Omega \mathcal{C}\underline{\boldsymbol{\epsilon}}(\boldsymbol{u}):\underline{\boldsymbol{\epsilon}}(\boldsymbol{\psi})+\int_\Omega \boldsymbol{f}\cdot\boldsymbol{\psi}+\int_{\Gamma_N}\boldsymbol{\sigma}_N\cdot\boldsymbol{\psi}, \tag{5c}$$

for all $(\boldsymbol{\phi},\boldsymbol{\psi})$ test functions in $\mathcal{T}$. Since this is a weak formulation of the first two equations of elastodynamics (2), a standard argument shows that equation (5a) gives the equation (2a), and that equation (5c) gives the equation (2b) as well as equation (2d). The equation (2c) is automatically satisfied by the definition of the phase manifold $\mathcal{M}$. This shows that the equations (2) define a Hamiltonian dynamical system.

Let us now consider the case in which the data $\boldsymbol{f}$, $\boldsymbol{\sigma}_N$ and $\boldsymbol{u}_D$ do depend on time. In this case, a direct differentiation with respect to time gives that

$$\dot{H}(u(t),v(t),t)=-\int_\Omega \dot{\boldsymbol{f}}(t)\cdot\boldsymbol{u}(t)-\int_{\Gamma_N}\dot{\boldsymbol{\sigma}}_N(t)\cdot\boldsymbol{u}(t)+\int_{\Gamma_D}\dot{\boldsymbol{u}}_D(t)\cdot(\mathcal{C}\underline{\boldsymbol{\epsilon}}(\boldsymbol{u}(t))\boldsymbol{n}). \tag{6}$$

Hence, it is necessary to have the data independent of time for the equations of elastodynamics to be a Hamiltonian dynamical system. Since we are interested in the case in which the Hamiltonian is constant in time, in view of the above identity, in the remaining of the paper, we assume that the data $\boldsymbol{u}_D$, $\boldsymbol{f}$ and $\boldsymbol{\sigma}_N$ are **independent of time**. Of course, all the schemes we consider can be trivially extended to the case in which the data depend on time.

2.2. Conservation laws

We next state the classical conservation laws of linear elastodynamics for the linear and angular momenta, and the energy. We show that they are a direct consequence of the fact that, if $J = J(\boldsymbol{u}(t), \boldsymbol{v}(t))$ is a functional defined on the orbits $t \mapsto (\boldsymbol{u}(t), \boldsymbol{v}(t))$ of a Hamiltonian dynamical system, then

$$\dot{J} = \{J, H\}. \tag{7}$$

Proposition 2.1. *Let $(\boldsymbol{u}, \boldsymbol{v})$ be any solution of the boundary-value problem* (2)*. Then the linear momentum $\boldsymbol{I}(\boldsymbol{v}) = \int_\Omega \rho\, \boldsymbol{v}$, the angular momentum $\boldsymbol{J}(\boldsymbol{v}) = \int_\Omega \boldsymbol{x} \times \rho\, \boldsymbol{v}$, and the total energy $E(\boldsymbol{u}, \boldsymbol{v}) = \int_\Omega \left(\frac{1}{2}\rho\, \boldsymbol{v}\cdot\boldsymbol{v} + \frac{1}{2}\,\mathcal{C}\underline{\boldsymbol{\epsilon}}(\boldsymbol{u}) : \underline{\boldsymbol{\epsilon}}(\boldsymbol{u})\right)$ are constant in time whenever $\Gamma_D = \emptyset$, and $\boldsymbol{f}$ and $\boldsymbol{\sigma}_N$ are zero.*

Proof. These conservation laws can be deduced by using the Hamiltonian structure of the equations in question. Indeed, by (7), to show that the functional $J = J(\boldsymbol{u}, \boldsymbol{v})$ is constant in time, we only have to show that $\{J, H\} = 0$.

Take $J := \boldsymbol{\eta} \cdot \boldsymbol{I}(\boldsymbol{v})$ where $\boldsymbol{\eta}$ is any three-dimensional constant vector. Then, since $\Gamma_D = \emptyset$, we have that $\mathcal{T} = \mathcal{C}^\infty(\Omega) \times \mathcal{C}^\infty(\Omega)$ and we can write that $J = C_{\boldsymbol{v}}(\boldsymbol{\psi})$ where $\boldsymbol{\psi} = \boldsymbol{\eta}$. As a consequence, $\{J, H\} = 0$ by the equation (5c) and the fact $\boldsymbol{\eta}$ is a constant vector. Since the vector $\boldsymbol{\eta}$ was arbitrary, this proves the conservation of the first quantity in time.

Now, take $J := \boldsymbol{\eta} \cdot \boldsymbol{J}(\boldsymbol{v})$ where $\boldsymbol{\eta}$ is again any three-dimensional constant vector. Then, by a similar argument, we see that $J = C_{\boldsymbol{v}}(\boldsymbol{\psi})$ where $\boldsymbol{\psi} = \boldsymbol{\eta} \times \boldsymbol{x}$. As a consequence, $\{J, H\} = 0$ by the equation (5c) and the fact $\boldsymbol{\eta}$ is a constant vector. Since the vector $\boldsymbol{\eta}$ was arbitrary, this proves the conservation of the second quantity.

Finally, for $J := E$, the conservation in time follows from the fact that, when $\boldsymbol{f}$ and $\boldsymbol{\sigma}_N$ are zero, $E = H$ and from the fact that $\{H, H\} = 0$, by the antisymmetry of the Poisson bracket.

This completes the proof. $\square$

3. The semidiscrete Finite element methods

In this section, we describe the finite element methods we are going to consider for the space discretization of the equations of elastodynamics. So, after introducing the notation, we describe the semidiscrete method for mixed methods, and for both the HDG and DG methods. For simplicity, we restrict our attention to methods using symmetric approximate stresses. We end by describing the HDG method we are going to use in our numerical results.

3.1. Notation

Let $\mathcal{T}_h = \{K\}$, for $0 < h < 1$, be a family of conforming triangulations of $\overline{\Omega}$. Let h_K be the inner diameter of an element K in $\mathcal{T}_h$ and we define by h the maximum over the elements.

We assume that the triangulation $\mathcal{T}_h$ is shape-regular, see [10], and define the following sets

$\partial\mathcal{T}_h$: the set of ∂K for all elements K of the triangulation Th,

$\mathcal{F}_h$: the set of all the faces of the triangulation $\mathcal{T}_h$,

$\mathcal{F}_h^0$: the set of the interior faces of the triangulation $\mathcal{T}_h$,

$\mathcal{F}_h^N$: the set of faces lying on the boundary Γ_N,

$\mathcal{F}_h^D$: the set of faces on the boundary Γ_D.

Now we introduce some notation for inner products. Let $D \in \mathbb{R}^d$, we denote by $(\cdot,\cdot)_D$ the inner product for vectors $\boldsymbol{w}, \boldsymbol{v} \in [L^2(D)]^d$ and tensors $\underline{\boldsymbol{\chi}}, \underline{\boldsymbol{\sigma}} \in [L^2(D)]^{d\times d}$, that is,

$$(\boldsymbol{w},\boldsymbol{v})_D = \int_D \boldsymbol{w}\cdot\boldsymbol{v}, \quad (\underline{\boldsymbol{\chi}},\underline{\boldsymbol{\sigma}})_D = \int_D \underline{\boldsymbol{\chi}} : \underline{\boldsymbol{\sigma}}.$$

Similar definitions for the inner products in $(d-1)$-dimensional domains are considered. Then, we define the inner products over the triangulation $\mathcal{T}_h$ and the sets of boundary and faces of $\mathcal{T}_h$

$$\begin{aligned}
(\underline{\boldsymbol{\chi}},\underline{\boldsymbol{\sigma}})_{\mathcal{T}_h} &= \sum_{K\in\mathcal{T}_h} (\underline{\boldsymbol{\chi}},\underline{\boldsymbol{\sigma}})_K, \quad &(\boldsymbol{w},\boldsymbol{v})_{\mathcal{T}_h} &= \sum_{K\in\mathcal{T}_h} (\boldsymbol{w},\boldsymbol{v})_K \\
\langle \boldsymbol{w},\boldsymbol{v}\rangle_{\mathcal{E}} &= \sum_{F\in\mathcal{E}} \langle \boldsymbol{w},\boldsymbol{v}\rangle_F, \quad &\langle \boldsymbol{w},\boldsymbol{v}\rangle_{\partial\mathcal{T}_h} &= \sum_{K\in\mathcal{T}_h} \langle \boldsymbol{w},\boldsymbol{v}\rangle_{\partial K}
\end{aligned}$$

where $\mathcal{E}$ denotes a collection of faces, for instance $\mathcal{E} = \partial K, \mathcal{F}_h, \mathcal{F}_h^0, \mathcal{F}_h^D, \mathcal{F}_h^N$.

Furthermore, we introduce some standard discontinuous Galerkin notation for the averages and jumps over faces. For an interior face $F \in \mathcal{F}_h^0$, we have two elements K^- and K^+ such that $F = \partial K^+ \cap \partial K^-$, and denoting the trace of a scalar, vector, or tensor valued function ϕ to the boundary of $K^\pm$ by $\phi^\pm$. Then, we define the average and jump on $F \in \mathcal{F}_h$ of a vector function $\boldsymbol{w}$ *and* its exterior trace $\boldsymbol{w}^{ext}$ by

$$\begin{aligned}
\{\!\{\boldsymbol{w}\}\!\} &:= \begin{cases} \frac{1}{2}(\boldsymbol{w}^+ + \boldsymbol{w}^-) & \text{if } F\in\mathcal{F}_h^0, \\ \boldsymbol{w} & \text{if } F \in \mathcal{F}_h^D \cup \mathcal{F}_h^N, \end{cases} \\
[\![\boldsymbol{w}\otimes\boldsymbol{n}]\!] &:= \begin{cases} \boldsymbol{w}^+\otimes\boldsymbol{n}^+ + \boldsymbol{w}^-\otimes\boldsymbol{n}^- & \text{if } F\in\mathcal{F}_h^0, \\ \boldsymbol{w}\otimes\boldsymbol{n} \quad - \boldsymbol{w}^{ext}\otimes\boldsymbol{n} & \text{if } F \in \mathcal{F}_h^D \cup \mathcal{F}_h^N. \end{cases}
\end{aligned}$$

We take as the exterior trace $\boldsymbol{w}^{ext}$ a boundary data. For example, on Γ_D, we take $\boldsymbol{u}_h^{ext} := \boldsymbol{u}_D$. There is no need to define the exterior trace on Γ_N.

Similarly, we define the average and jump on $F \in \mathcal{F}_h$ of a tensor function $\underline{\boldsymbol{\chi}}$ and its exterior trace $\underline{\boldsymbol{\chi}}^{ext}$ by

$$\begin{aligned}
\{\!\{\underline{\boldsymbol{\chi}}\}\!\} &:= \begin{cases} \frac{1}{2}(\underline{\boldsymbol{\chi}}^+ + \underline{\boldsymbol{\chi}}^-) & \text{if } F\in\mathcal{F}_h^0, \\ \underline{\boldsymbol{\chi}} & \text{if } F \in \mathcal{F}_h^D \cup \mathcal{F}_h^N. \end{cases} \\
[\![\underline{\boldsymbol{\chi}}\,\boldsymbol{n}]\!] &:= \begin{cases} \underline{\boldsymbol{\chi}}^+\boldsymbol{n}^+ + \underline{\boldsymbol{\chi}}^-\boldsymbol{n}^-, & \text{if } F\in\mathcal{F}_h^0 \\ \underline{\boldsymbol{\chi}}\boldsymbol{n} \quad - \underline{\boldsymbol{\chi}}^{ext}\boldsymbol{n} & \text{if } F \in \mathcal{F}_h^D \cup \mathcal{F}_h^N. \end{cases}
\end{aligned}$$

We take as the exterior trace $\underline{\boldsymbol{\chi}}\,\boldsymbol{n}$ a boundary data. For example, on Γ_N, we take $\underline{\boldsymbol{\sigma}}_h^{ext} := \boldsymbol{\sigma}_N$. There is no need to define the exterior trace on Γ_D.

Next, we define the finite element space for symmetric tensors, and the space for vectors by

$$\underline{\boldsymbol{V}}_h^M = \{\underline{\boldsymbol{\chi}} \in [L^2(\Omega)]^{d\times d} \cap \mathbb{S},], \nabla\cdot\underline{\boldsymbol{\chi}} \in [L^2(\Omega)]^d : \underline{\boldsymbol{\chi}}|_K \in \underline{\boldsymbol{V}}(K), \forall K \in \mathcal{T}_h\}, \quad (8a)$$

$$\underline{\boldsymbol{V}}_h = \{\underline{\boldsymbol{\chi}} \in [L^2(\Omega)]^{d\times d} \cap \mathbb{S} : \underline{\boldsymbol{\chi}}|_K \in \underline{\boldsymbol{V}}(K), \forall K \in \mathcal{T}_h\}, \quad (8b)$$

$$\boldsymbol{W}_h = \{\boldsymbol{w} \in [L^2(\Omega)]^d : \boldsymbol{w}|_K \in \boldsymbol{W}(K), \forall K \in \mathcal{T}_h\}, \quad (8c)$$

where $\underline{\boldsymbol{V}}(K)$ and $\boldsymbol{W}(K)$ are local finite element spaces which determine the numerical method. By $\mathbb{S}$ we denote the set of symmetric-valued matrices.

3.2. Mixed finite element methods

3.2.1. For steady-state

The mixed methods for the steady-state problem

$$-\nabla\cdot(\underline{\boldsymbol{\sigma}}) = \boldsymbol{f}, \quad \mathcal{A}\underline{\boldsymbol{\sigma}} = \underline{\boldsymbol{\epsilon}}(\boldsymbol{u}) \text{ in } \Omega, \quad \boldsymbol{u} = \boldsymbol{u}_D \text{ on } \Gamma_D, \text{ and } \underline{\boldsymbol{\sigma}}\boldsymbol{n} = \boldsymbol{\sigma}_N \text{ on } \Gamma_N,$$

seek approximations of $(\boldsymbol{u}, \underline{\boldsymbol{\sigma}})$, $(\boldsymbol{u}_h, \underline{\boldsymbol{\sigma}}_h)$, in the space $\boldsymbol{W}_h \times \underline{\boldsymbol{V}}_{h,\boldsymbol{\sigma}_N}^M$, where

$$\underline{\boldsymbol{V}}_{h,\boldsymbol{\sigma}_N}^M = \{\underline{\boldsymbol{\chi}} \in \underline{\boldsymbol{V}}_h^M : \underline{\boldsymbol{\chi}}\boldsymbol{n} = \boldsymbol{\sigma}_N \text{ on } \Gamma_N\}.$$

They are determined as the solution of

$$-(\nabla\cdot\underline{\boldsymbol{\sigma}}_h, \boldsymbol{w})_{\mathcal{T}_h} = (\boldsymbol{f}, \boldsymbol{w})_{\mathcal{T}_h} \qquad \forall\, \boldsymbol{w} \in \boldsymbol{W}_h, \quad (9a)$$

$$(\mathcal{A}\,\underline{\boldsymbol{\sigma}}_h, \underline{\boldsymbol{\chi}})_{\mathcal{T}_h} + (\boldsymbol{u}_h, \nabla\cdot\underline{\boldsymbol{\chi}})_{\mathcal{T}_h} = \langle \boldsymbol{u}_D, \underline{\boldsymbol{\chi}}\boldsymbol{n}\rangle_{\Gamma_D} \quad \forall\, \underline{\boldsymbol{\chi}} \in \underline{\boldsymbol{V}}_{h,\boldsymbol{0}}^M. \quad (9b)$$

Here $\mathcal{A} = \mathcal{C}^{-1}$ is the compliance tensor. Examples of these mixed methods can be found in [8, 2, 7, 19, 20].

3.2.2. The semidiscrete scheme

We define the semidiscrete scheme in a way which will be suitable to uncovering its Hamiltonian structure. Thus, the semidiscrete scheme defines the approximation to $(\boldsymbol{u}(t), \boldsymbol{v}(t))$, $(\boldsymbol{u}_h(t), \boldsymbol{v}_h(t))$, as the element of the space $\boldsymbol{W}_h \times \boldsymbol{W}_h$ satisfying the equations

$$(\dot{\boldsymbol{u}}_h(t), \boldsymbol{w})_{\mathcal{T}_h} = (\boldsymbol{v}_h(t), \boldsymbol{w})_{\mathcal{T}_h} \qquad \forall\, \boldsymbol{w} \in \boldsymbol{W}_h, \quad (10a)$$

$$(\rho\,\dot{\boldsymbol{v}}_h(t), \boldsymbol{w})_{\mathcal{T}_h} = (\nabla\cdot\underline{\boldsymbol{\sigma}}_h(t), \boldsymbol{w})_{\mathcal{T}_h} + (\boldsymbol{f}, \boldsymbol{w})_{\mathcal{T}_h} \quad \forall\, \boldsymbol{w} \in \boldsymbol{W}_h, \quad (10b)$$

where $\underline{\boldsymbol{\sigma}}_h(t)$ is the element of $\underline{\boldsymbol{V}}_{h,\boldsymbol{\sigma}_N}^M$ which solves the equation

$$(\mathcal{A}\underline{\boldsymbol{\sigma}}_h(t), \underline{\boldsymbol{\chi}})_{\mathcal{T}_h} + (\boldsymbol{u}_h(t), \nabla\cdot\underline{\boldsymbol{\chi}})_{\mathcal{T}_h} = \langle \boldsymbol{u}_D, \underline{\boldsymbol{\chi}}\boldsymbol{n}\rangle_{\Gamma_D} \qquad \forall\, \underline{\boldsymbol{\chi}} \in \underline{\boldsymbol{V}}_{h,\boldsymbol{0}}^M. \quad (10c)$$

We complete the definition of the scheme by setting the initial condition as follows:

$$(\boldsymbol{u}_h(0), \boldsymbol{v}(0)) := (\Pi(\boldsymbol{u}_0), P(\boldsymbol{v}_0)),$$

for some projections Π, P into $\boldsymbol{W}_h$.

To be able to define the Hamiltonian for this semidiscrete scheme in the case in which $\boldsymbol{\sigma}_N$ is not zero, we must introduce an approximation to $\boldsymbol{u}(t)|_{\Gamma_N}$. So, we take $\widehat{\boldsymbol{u}}_h(t)$ as the element of $\{\underline{\boldsymbol{\chi}}\boldsymbol{n}|_{\Gamma_N} : \underline{\boldsymbol{\chi}} \in \underline{\boldsymbol{V}}_h^M\}$ which solves the equation

$$\langle \widehat{\boldsymbol{u}}_h(t), \underline{\boldsymbol{\chi}}\boldsymbol{n}\rangle_{\Gamma_N} = (\mathcal{A}\underline{\boldsymbol{\sigma}}_h(t), \underline{\boldsymbol{\chi}})_{\mathcal{T}_h} + (\boldsymbol{u}_h(t), \nabla\cdot\underline{\boldsymbol{\chi}})_{\mathcal{T}_h} - \langle \boldsymbol{u}_D, \underline{\boldsymbol{\chi}}\boldsymbol{n}\rangle_{\Gamma_D} \qquad \forall\, \underline{\boldsymbol{\chi}} \in \underline{\boldsymbol{V}}_h^M. \tag{11}$$

Using the fact that $\underline{\boldsymbol{\sigma}}_h$ and $\boldsymbol{u}_h$ solve the equation (10c), it is not difficult to show that $\widehat{\boldsymbol{u}}_h(t)$ is well defined. Moreover, the function $\widehat{\boldsymbol{u}}_h(t)$ can be computed in a face-by-face manner.

3.3. *The HDG and DG semidiscrete methods*

3.3.1. *For steady-state*

The HDG and DG methods for the steady-state problem

$$-\nabla\cdot(\underline{\boldsymbol{\sigma}}) = \boldsymbol{f}, \quad \underline{\boldsymbol{\sigma}} = \mathcal{C}\underline{\boldsymbol{\epsilon}}(\boldsymbol{u}) \quad \text{in } \Omega, \quad \boldsymbol{u} = \boldsymbol{u}_D \quad \text{on } \Gamma_D, \quad \text{and} \quad \underline{\boldsymbol{\sigma}}\boldsymbol{n} = \boldsymbol{\sigma}_N \quad \text{on } \Gamma,$$

define $(\boldsymbol{u}_h, \underline{\boldsymbol{\sigma}}_h, \underline{\boldsymbol{\epsilon}}_h)$ as the solution of

$$(\underline{\boldsymbol{\sigma}}_h, \nabla\boldsymbol{w})_K - \langle \widehat{\underline{\boldsymbol{\sigma}}}_h\boldsymbol{n}, \boldsymbol{w}\rangle_{\partial K} = (\boldsymbol{f}, \boldsymbol{w})_K \quad \forall \boldsymbol{w} \in \boldsymbol{W}(K), \tag{12a}$$

$$(\underline{\boldsymbol{\sigma}}_h, \underline{\boldsymbol{\chi}})_K - (\mathcal{C}\,\underline{\boldsymbol{\epsilon}}_h, \underline{\boldsymbol{\chi}})_K = 0 \quad \forall \underline{\boldsymbol{\chi}} \in \underline{\boldsymbol{V}}(K), \tag{12b}$$

$$(\underline{\boldsymbol{\epsilon}}_h, \underline{\boldsymbol{\chi}})_K + (\boldsymbol{u}_h, \nabla\cdot\underline{\boldsymbol{\chi}})_K - \langle \widehat{\boldsymbol{u}}_h, \underline{\boldsymbol{\chi}}\boldsymbol{n}\rangle_{\partial K} = 0 \quad \forall \underline{\boldsymbol{\chi}} \in \underline{\boldsymbol{V}}(K). \tag{12c}$$

The definition of the method is completed by the choice of the local finite element spaces $\underline{\boldsymbol{V}}(K)$ and $\boldsymbol{W}(K)$, and by the definition of the numerical traces $\widehat{\underline{\boldsymbol{\sigma}}}_h\boldsymbol{n}$ and $\widehat{\boldsymbol{u}}_h$.

For the HDG methods, the numerical trace $\widehat{\boldsymbol{u}}_h$ is a new variable and $\widehat{\underline{\boldsymbol{\sigma}}}_h$ is given by

$$\widehat{\underline{\boldsymbol{\sigma}}}_h\boldsymbol{n} = \underline{\boldsymbol{\sigma}}_h\boldsymbol{n} - \tau(P_{\boldsymbol{M}}\boldsymbol{u}_h - \widehat{\boldsymbol{u}}_h) \qquad \text{on } \partial\mathcal{T}_h, \tag{13}$$

where τ is the so-called stabilization function which we take to be constant on each face of ∂K for any $K \in \mathcal{T}_h$. When the operator $P_{\boldsymbol{M}}$ in (13) is not the identity, it is L^2 projection onto the space $\boldsymbol{M}_h$. In this case the resulting stabilization is usually called the Leherenfled-Schöberl stabilization, see [26, Remark 1.2.4] and [27].

The numerical trace $\widehat{\boldsymbol{u}}_h$ lies in the space

$$\boldsymbol{M}_h = \{\mu \in L^2(\mathcal{F}_h)^d : \mu|_F \in \boldsymbol{M}(F), \forall F \in \mathcal{F}_h\},$$

and is defined as the solution of

$$\langle \widehat{\underline{\boldsymbol{\sigma}}}_h\boldsymbol{n},\, \boldsymbol{\mu}\rangle_{\partial\mathcal{T}_h\setminus\Gamma_D} = \langle \boldsymbol{\sigma}_N,\, \boldsymbol{\mu}\rangle_{\Gamma_N},$$
$$\langle \widehat{\boldsymbol{u}}_h,\, \boldsymbol{\mu}\rangle_{\Gamma_D} = \langle \boldsymbol{u}_D,\, \boldsymbol{\mu}\rangle_{\Gamma_D}$$

for all $\boldsymbol{\mu} \in \boldsymbol{M}_h$. Examples of these methods can be found in [40, 41, 32, 31, 12, 34].

For the DG methods, the numerical traces are defined by

$$\widehat{\underline{\boldsymbol{\sigma}}}_h = \begin{cases} \{\!\{\underline{\boldsymbol{\sigma}}_h\}\!\} + C_{11}[\![\boldsymbol{u}_h \otimes \boldsymbol{n}]\!] - [\![\underline{\boldsymbol{\sigma}}_h \boldsymbol{n}]\!] \otimes \boldsymbol{C}_{12} & \text{if } F \in \mathcal{F}_h^0, \\ \underline{\boldsymbol{\sigma}}_h + C_{11}[\![\boldsymbol{u}_h \otimes \boldsymbol{n}]\!] & \text{if } F \in \mathcal{F}_h^D, \\ \boldsymbol{\sigma}_N & \text{if } F \in \mathcal{F}_h^N, \end{cases} \tag{14a}$$

$$\widehat{\boldsymbol{u}}_h = \begin{cases} \{\!\{\boldsymbol{u}_h\}\!\} + [\![\boldsymbol{u}_h \otimes \boldsymbol{n}]\!] \cdot \boldsymbol{C}_{12} + C_{22}[\![\underline{\boldsymbol{\sigma}}_h \boldsymbol{n}]\!] & \text{if } F \in \mathcal{F}_h^0, \\ \boldsymbol{u}_D & \text{if } F \in \mathcal{F}_h^D, \\ \boldsymbol{u}_h + C_{22}(\underline{\boldsymbol{\sigma}}_h \boldsymbol{n} - \boldsymbol{\sigma}_N) & \text{if } F \in \mathcal{F}_h^N. \end{cases} \tag{14b}$$

An example is the DG method proposed in [14]. When $C_{22} = 0$, the method is called an LDG method. Some of these DG methods can become HDG methods when the parameters $C_{11}, \boldsymbol{C}_{12}$ and C_{22} are suitably defined as was shown in [11] in the framework of steady-state diffusion.

3.3.2. Semidiscrete schemes

The HDG and DG schemes approximate $(\boldsymbol{u}(t), \boldsymbol{v}(t))$ by the element $(\boldsymbol{u}_h(t), \boldsymbol{v}_h(t))$ of $\boldsymbol{W}_h \times \boldsymbol{W}_h$ which solves the equations

$$(\dot{\boldsymbol{u}}_h(t), \boldsymbol{w})_{\mathcal{T}_h} = (\boldsymbol{v}_h(t), \boldsymbol{w})_{\mathcal{T}_h} \qquad \forall\, \boldsymbol{w} \in \boldsymbol{W}_h, \tag{15a}$$

$$(\rho\, \dot{\boldsymbol{v}}_h(t), \boldsymbol{w})_{\mathcal{T}_h} = -(\underline{\boldsymbol{\sigma}}_h(t), \nabla \boldsymbol{w})_{\mathcal{T}_h} + (\boldsymbol{f}, \boldsymbol{w})_{\mathcal{T}_h} + \langle \widehat{\underline{\boldsymbol{\sigma}}}_h(t)\boldsymbol{n}, \boldsymbol{w}\rangle_{\partial\mathcal{T}_h} \quad \forall\, \boldsymbol{w} \in \boldsymbol{W}_h, \tag{15b}$$

where $(\underline{\boldsymbol{\epsilon}}_h(t), \underline{\boldsymbol{\sigma}}_h(t))$ is the element of $\underline{\boldsymbol{V}}_h \times \underline{\boldsymbol{V}}_h$ solution of

$$(\underline{\boldsymbol{\epsilon}}_h(t), \underline{\boldsymbol{\chi}})_{\mathcal{T}_h} + (\boldsymbol{u}_h(t), \nabla\cdot \underline{\boldsymbol{\chi}})_{\mathcal{T}_h} - \langle \widehat{\boldsymbol{u}}_h(t), \underline{\boldsymbol{\chi}}\boldsymbol{n}\rangle_{\partial\mathcal{T}_h} = 0 \quad \forall \underline{\boldsymbol{\chi}} \in \underline{\boldsymbol{V}}_h, \tag{15c}$$

$$(\underline{\boldsymbol{\sigma}}_h(t), \underline{\boldsymbol{\chi}})_{\mathcal{T}_h} - (\mathcal{C}\, \underline{\boldsymbol{\epsilon}}_h(t), \underline{\boldsymbol{\chi}})_{\mathcal{T}_h} = 0 \quad \forall \underline{\boldsymbol{\chi}} \in \underline{\boldsymbol{V}}_h, \tag{15d}$$

and $\widehat{\boldsymbol{u}}_h(t)$ is the element of $\boldsymbol{M}_h$ which solves

$$\langle \widehat{\underline{\boldsymbol{\sigma}}}_h(t)\boldsymbol{n},\, \boldsymbol{\mu}\rangle_{\partial\mathcal{T}_h\setminus\Gamma_D} = \langle \boldsymbol{\sigma}_N,\, \boldsymbol{\mu}\rangle_{\Gamma_N} \tag{15e}$$

$$\langle \widehat{\boldsymbol{u}}_h(t),\, \boldsymbol{\mu}\rangle_{\Gamma_D} = \langle \boldsymbol{u}_D,\, \boldsymbol{\mu}\rangle_{\Gamma_D}, \tag{15f}$$

for all $\boldsymbol{\mu} \in \boldsymbol{M}_h$. The initial condition is of the form

$$(\boldsymbol{u}_h(0), \boldsymbol{v}(0)) := (\Pi(\boldsymbol{u}_0), P(\boldsymbol{v}_0)),$$

for some projections Π, P into $\boldsymbol{W}_h$. To complete the scheme, the numerical traces $\widehat{\boldsymbol{u}}_h(t)$ and $\widehat{\underline{\boldsymbol{\sigma}}}_h(t)\boldsymbol{n}$ are chosen as described in the previous subsection.

3.4. The HDG$_k$+ semidiscrete scheme

To end this section, we describe the HDG method we are going to use in our numerical experiments. It is denoted by HDG$_k$+ and uses the local spaces introduced in [35], namely,

$$\underline{\boldsymbol{V}}(K) = [\mathbb{P}^k(K)]^{d\times d} \cap \mathbb{S}, \quad \boldsymbol{W}(K) = [\mathbb{P}^{k+1}(K)]^d, \quad \boldsymbol{M}(F) = [\mathbb{P}^k(F)]^d. \tag{16}$$

for any element $K \in \mathcal{T}_h$ and face $F \in \mathcal{F}_h$.

To be able to prove optimal error estimates, we take the initial data $\boldsymbol{u}_h(0)$ as the first component of the approximate solution $(\boldsymbol{u}_h(0), \underline{\boldsymbol{\epsilon}}_h(0), \underline{\boldsymbol{\sigma}}_h(0))$ given by the HDG$_k$+ method applied to

$$\begin{aligned} -\nabla\cdot\underline{\boldsymbol{\sigma}}(0) = -\nabla\cdot(\mathcal{C}\,\underline{\boldsymbol{\epsilon}}(\boldsymbol{u}_0)), \qquad \underline{\boldsymbol{\sigma}}(0) = \mathcal{C}\,\underline{\boldsymbol{\epsilon}}(0) \quad \text{in } \Omega,\\ \boldsymbol{u}(0) = \boldsymbol{u}_D \quad \text{on } \Gamma_D, \quad \underline{\boldsymbol{\sigma}}(0)\boldsymbol{n} \;= \boldsymbol{\sigma}_N \quad \text{on } \Gamma_N. \end{aligned}$$

The initial approximation of the velocity $\boldsymbol{v}_h(0)$ is taken as the L^2-projection onto the space $\boldsymbol{W}_h$ of $\boldsymbol{v}_0$.

We also need to assume that the following elliptic regularity condition

$$\|\boldsymbol{\Phi}\|_{H^2(\Omega)^d} + \|\mathcal{C}\underline{\boldsymbol{\epsilon}}(\boldsymbol{\Phi})\|_{H^1(\Omega)^{d\times d}} \leq C_{\text{reg}}\|\nabla\cdot(\mathcal{C}\underline{\boldsymbol{\epsilon}}(\boldsymbol{\Phi}))\|_{L^2(\Omega)^d}, \tag{17}$$

holds for any $\boldsymbol{\Phi} \in H^1(\Omega)^d$ and finite right-hand side of the above inequality.

Theorem 3.1. *We have, for $k \geq 1$,*

$$\|\mathcal{C}(\underline{\boldsymbol{\epsilon}}(T) - \underline{\boldsymbol{\epsilon}}_h(T))\|_{L^2(\Omega)^{d\times d}} + \|\rho(\boldsymbol{v} - \boldsymbol{v}_h)\|_{L^2(\Omega)^d} \leq C\,\Theta\, h^m(1+T),$$

for $1 \leq m \leq k$, where $\Theta := \sum_{i=0}^{3}\sup_{t\in[0,T]}\big(\|\underline{\boldsymbol{\sigma}}^{(i)}\|_{H^m(\Omega)^{d\times d}} + \|\boldsymbol{u}^{(i)}\|_{H^{m+1}(\Omega)^d}\big)$.
Moreover, if the elliptic regularity inequality (17) *holds, then*

$$\|\boldsymbol{u}(T) - \boldsymbol{u}_h(T)\|_{L^2(\Omega)^d} \leq C\Theta\, h^{m+1}(1+T),$$

for $1 \leq m \leq k+1$.

The proof of this result is extremely similar to that provided in [15] for a related scheme. Indeed, in [15], new techniques were provided for the analysis of an HDG$_k$+ method proposed in [35] for the equations of linear elasticity. These techniques were used to analyze the semidiscrete scheme resulting from the space discretization of the equations of elastodynamics (formulated with a second order-time derivative and with the compliance tensor) by the HDG$_k$+ method.

This new analysis allows to simplify the quasi uniformity assumption on the mesh of the original paper [35]. The main differences between the semidiscrete scheme in [15] and the scheme under consideration is that they use a formulation with two time derivatives whereas we use a first-order system, and that they use the the compliance tensor $\mathcal{A} = \mathcal{C}^{-1}$ whereas we use the stiffness tensor $\mathcal{C}$ tensor. When both tensors are well defined, the differences between these two formulations are really minor and can even produce *superclose* approximate solutions, as proved in [13] for the steady-state diffusion problem.

4. The Hamiltonian structure of the semidiscrete methods

In this section we present the main results. We prove that, under space discretization by the mixed, DG and HDG methods, the resulting dynamical system is Hamiltonian. We do this in two equivalent ways. In Section 4.1, we use the approach using Poisson brackets sketched in Section 2, and in Section 4.2, the canonical approach for finite dimensional ODEs. We end in Section 4.3, by proving the conservation properties of the semidiscrete schemes.

4.1. The Poisson brackets approach

We prove the Hamiltonian structure of the semidiscrete schemes by using the approach sketched in Section 2. Indeed, we claim that the three semidiscrete methods define a Hamiltonian dynamical system for which

(i) the phase space is $\mathcal{M}_h = \boldsymbol{W}_h \times \boldsymbol{W}_h$,

(ii) the Poisson bracket is

$$\{F, G\}_h = (\rho^{-1}\frac{\delta F}{\delta \boldsymbol{u}_h}, \frac{\delta G}{\delta \boldsymbol{v}_h})_{\mathcal{T}_h} - (\rho^{-1}\frac{\delta F}{\delta \boldsymbol{v}_h}, \frac{\delta G}{\delta \boldsymbol{u}_h})_{\mathcal{T}_h}.$$

(iii) The Hamiltonians, for each of the methods, are

$$\begin{aligned}
H_h^{M}(\boldsymbol{u}_h, \boldsymbol{v}_h) &= \frac{1}{2}\left((\rho \boldsymbol{v}_h, \boldsymbol{v}_h)_{\mathcal{T}_h} + (\mathcal{A}\,\boldsymbol{\sigma}_h, \boldsymbol{\sigma}_h)_{\mathcal{T}_h}\right) - (\boldsymbol{f}, \boldsymbol{u}_h)_{\mathcal{T}_h} - \langle \boldsymbol{\sigma}_N, \widehat{\boldsymbol{u}}_h\rangle_{\mathcal{F}_h^N},\\
H_h^{HDG}(\boldsymbol{u}_h, \boldsymbol{v}_h) &= \frac{1}{2}\left((\rho \boldsymbol{v}_h, \boldsymbol{v}_h)_{\mathcal{T}_h} + (\,\mathcal{C}\,\underline{\boldsymbol{\epsilon}}_h, \underline{\boldsymbol{\epsilon}}_h\,)_{\mathcal{T}_h}\right) - (\boldsymbol{f}, \boldsymbol{u}_h)_{\mathcal{T}_h} - \langle \boldsymbol{\sigma}_N, \widehat{\boldsymbol{u}}_h\rangle_{\mathcal{F}_h^N}\\
&\quad + \frac{1}{2}\langle \tau(P_{\boldsymbol{M}}\boldsymbol{u}_h - \widehat{\boldsymbol{u}}_h), P_{\boldsymbol{M}}\boldsymbol{u}_h - \widehat{\boldsymbol{u}}_h\rangle_{\partial\mathcal{T}_h},\\
H_h^{DG}(\boldsymbol{u}_h, \boldsymbol{v}_h) &= \frac{1}{2}\left((\rho \boldsymbol{v}_h, \boldsymbol{v}_h)_{\mathcal{T}_h} + (\,\mathcal{C}\,\underline{\boldsymbol{\epsilon}}_h, \underline{\boldsymbol{\epsilon}}_h\,)_{\mathcal{T}_h}\right) - (\boldsymbol{f}, \boldsymbol{u}_h)_{\mathcal{T}_h} - \langle \boldsymbol{\sigma}_N, \widehat{\boldsymbol{u}}_h\rangle_{\mathcal{F}_h^N}\\
&\quad - \frac{1}{2}C_{11}\langle [\![\boldsymbol{u}_h \otimes \boldsymbol{n}]\!], [\![\boldsymbol{u}_h \otimes \boldsymbol{n}]\!]\rangle_{\mathcal{F}_h^0 \cup \mathcal{F}_h^D}\\
&\quad - \frac{1}{2}C_{22}\langle [\![\underline{\boldsymbol{\sigma}}_h \boldsymbol{n}]\!], [\![\underline{\boldsymbol{\sigma}}_h \boldsymbol{n}]\!]\rangle_{\mathcal{F}_h^0 \cup \mathcal{F}_h^N},
\end{aligned}$$

(iv) the coordinates functionals are $C_{\boldsymbol{u}_h} = (\rho\, \boldsymbol{u}_h, \phi)_\Omega$ and $C_{\boldsymbol{v}_h} = (\rho\, \boldsymbol{v}_h, \psi)_\Omega$,

(v) the space of test functions is $\mathcal{T}_h = \boldsymbol{W}_h \times \boldsymbol{W}_h$.

Let us prove the claim.

4.1.1. The semidiscrete mixed method

Theorem 1 (Hamiltonian structure of the semidiscrete mixed methods). *The semidiscrete mixed finite element method* (10) *defines a Hamiltonian dynamical system.*

Proof. Using the definition of H_h^M, we get that

$$\delta H_h^M = (\delta \boldsymbol{v}_h, \rho\, \boldsymbol{v}_h)_{\mathcal{T}_h} + (\delta \underline{\boldsymbol{\sigma}}_h, \mathcal{A}\underline{\boldsymbol{\sigma}}_h)_{\mathcal{T}_h} - (\delta \boldsymbol{u}_h, \boldsymbol{f})_{\mathcal{T}_h} - \langle \delta \widehat{\boldsymbol{u}}_h, \boldsymbol{\sigma}_N\rangle_{\mathcal{F}_h^N}.$$

We now need to write the variations of $\underline{\boldsymbol{\sigma}}_h$ and $\widehat{\boldsymbol{u}}_h$ in terms of the variation of $\boldsymbol{u}_h$. So, by the equation (11) relating $\underline{\boldsymbol{\sigma}}_h$, $\widehat{\boldsymbol{u}}_h$ and $\boldsymbol{u}_h$, we have that

$$\langle \delta \widehat{\boldsymbol{u}}_h(t), \underline{\boldsymbol{\chi}}\boldsymbol{n}\rangle_{\Gamma_N} = (\mathcal{A}\delta\underline{\boldsymbol{\sigma}}_h(t), \underline{\boldsymbol{\chi}})_{\mathcal{T}_h} + (\delta \boldsymbol{u}_h(t), \nabla\cdot \underline{\boldsymbol{\chi}})_{\mathcal{T}_h} \qquad \forall\, \underline{\boldsymbol{\chi}} \in \underline{\boldsymbol{V}}_h^M,$$

and taking $\underline{\boldsymbol{\chi}} := \underline{\boldsymbol{\sigma}}_h$, we obtain

$$\langle \delta \widehat{\boldsymbol{u}}_h(t), \boldsymbol{\sigma}_N\rangle_{\Gamma_N} = (\mathcal{A}\delta\underline{\boldsymbol{\sigma}}_h(t), \underline{\boldsymbol{\sigma}}_h)_{\mathcal{T}_h} + (\delta \boldsymbol{u}_h(t), \nabla\cdot \underline{\boldsymbol{\sigma}}_h)_{\mathcal{T}_h},$$

This implies that

$$\delta H_h^M = (\delta \boldsymbol{v}_h, \rho \boldsymbol{v}_h)_{\mathcal{T}_h} - (\delta \boldsymbol{u}_h, \nabla\cdot \underline{\boldsymbol{\sigma}}_h)_{\mathcal{T}_h} - (\delta \boldsymbol{u}_h, \boldsymbol{f})_{\mathcal{T}_h}.$$

As a consequence, by the definition of the discrete Poisson bracket, we get that

$$\begin{aligned}
(\rho\, \dot{\boldsymbol{u}}_h, \boldsymbol{w})_{\mathcal{T}_h} &= \dot{C}_{\boldsymbol{u}_h}(\boldsymbol{w}) = \{C_{\boldsymbol{u}_h}(\boldsymbol{w}), H_h^M\}_h = (\frac{\delta H_h^M}{\delta \boldsymbol{v}_h}, \boldsymbol{w})_{\mathcal{T}_h} \quad = (\rho\, \boldsymbol{v}_h, \boldsymbol{w})_{\mathcal{T}_h},\\
(\rho\, \dot{\boldsymbol{v}}_h, \boldsymbol{w})_{\mathcal{T}_h} &= \dot{C}_{\boldsymbol{v}_h}(\boldsymbol{w}) = \{C_{\boldsymbol{v}_h}(\boldsymbol{w}), H_h^M\}_h = -(\frac{\delta H_h^M}{\delta \boldsymbol{u}_h}, \boldsymbol{w})_{\mathcal{T}_h} = (\nabla\cdot \underline{\boldsymbol{\sigma}}_h, \boldsymbol{w})_{\mathcal{T}_h}\\
&\qquad\qquad\qquad\qquad\qquad\qquad\qquad\qquad\qquad + (\boldsymbol{f}, \boldsymbol{w})_{\mathcal{T}_h},
\end{aligned}$$

for all $\boldsymbol{w} \in \boldsymbol{W}_h$. In other words, the equations defining the semidiscrete mixed methods define a Hamiltonian dynamical system. This completes the proof. □

4.1.2. The semidiscrete HDG method

Theorem 2 (Hamiltonian structure of the semidiscrete HDG methods). *The HDG method defined in* (15) *with numerical traces given by* (13) *defines a Hamiltonian dynamical system.*

Proof. Taking the variation of the functional H_h^{HDG}, we obtain

$$\begin{aligned}
\delta H_h^{HDG} = &(\rho \boldsymbol{v}_h, \delta \boldsymbol{v}_h)_{\mathcal{T}_h} + (\mathcal{C}\underline{\boldsymbol{\epsilon}}_h, \delta \underline{\boldsymbol{\epsilon}}_h)_{\mathcal{T}_h} - (\boldsymbol{f}, \delta \boldsymbol{u}_h)_{\mathcal{T}_h} - \langle \boldsymbol{\sigma}_N, \delta \widehat{\boldsymbol{u}}_h\rangle_{\mathcal{F}_h^N}\\
&+ \langle \tau(P_M \boldsymbol{u}_h - \widehat{\boldsymbol{u}}_h), \delta(P_M \boldsymbol{u}_h - \widehat{\boldsymbol{u}}_h)\rangle_{\partial\mathcal{T}_h}.
\end{aligned}$$

From equation (15d) with $\underline{\boldsymbol{\chi}} := \delta\underline{\boldsymbol{\epsilon}}_h$, we have that $(\mathcal{C}\underline{\boldsymbol{\epsilon}}_h, \delta\underline{\boldsymbol{\epsilon}}_h)_{\mathcal{T}_h} = (\underline{\boldsymbol{\sigma}}_h, \delta\underline{\boldsymbol{\epsilon}}_h)_{\mathcal{T}_h}$. If we now take the variation in equation (15c) and set $\underline{\boldsymbol{\chi}} := \underline{\boldsymbol{\sigma}}_h$, we obtain

$$(\mathcal{C}\underline{\boldsymbol{\epsilon}}_h, \delta\underline{\boldsymbol{\epsilon}}_h)_{\mathcal{T}_h} = -(\nabla\cdot\underline{\boldsymbol{\sigma}}_h, \delta \boldsymbol{u}_h)_{\mathcal{T}_h} + \langle \underline{\boldsymbol{\sigma}}_h \boldsymbol{n}, \delta\widehat{\boldsymbol{u}}_h\rangle_{\partial\mathcal{T}_h} = (\underline{\boldsymbol{\sigma}}_h, \nabla\delta\boldsymbol{u}_h)_{\mathcal{T}_h} - \langle \underline{\boldsymbol{\sigma}}_h\boldsymbol{n}, \delta(\boldsymbol{u}_h - \widehat{\boldsymbol{u}}_h)\rangle_{\partial\mathcal{T}_h}.$$

Hence, δH_h^{HDG} equals to

$$\begin{aligned}
&(\rho \boldsymbol{v}_h, \delta \boldsymbol{v}_h)_{\mathcal{T}_h} + (\underline{\boldsymbol{\sigma}}_h, \nabla\delta\boldsymbol{u}_h)_{\mathcal{T}_h} - \langle \underline{\boldsymbol{\sigma}}_h\boldsymbol{n}, \delta(\boldsymbol{u}_h - \widehat{\boldsymbol{u}}_h)\rangle_{\partial\mathcal{T}_h} - (\boldsymbol{f}, \delta \boldsymbol{u}_h)_{\mathcal{T}_h} - \langle \boldsymbol{\sigma}_N, \delta \widehat{\boldsymbol{u}}_h\rangle_{\mathcal{F}_h^N}\\
&\quad + \langle \tau(P_M \boldsymbol{u}_h - \widehat{\boldsymbol{u}}_h), \delta(P_M \boldsymbol{u}_h - \widehat{\boldsymbol{u}}_h)\rangle_{\partial\mathcal{T}_h}\\
&= (\rho \boldsymbol{v}_h, \delta \boldsymbol{v}_h)_{\mathcal{T}_h} + (\underline{\boldsymbol{\sigma}}_h, \nabla\delta\boldsymbol{u}_h)_{\mathcal{T}_h} - \langle \widehat{\underline{\boldsymbol{\sigma}}}_h\boldsymbol{n}, \delta(\boldsymbol{u}_h - \widehat{\boldsymbol{u}}_h)\rangle_{\partial\mathcal{T}_h} - (\boldsymbol{f}, \delta \boldsymbol{u}_h)_{\mathcal{T}_h} - \langle \boldsymbol{\sigma}_N, \delta \widehat{\boldsymbol{u}}_h\rangle_{\mathcal{F}_h^N}\\
&\quad + \langle \tau(P_M \boldsymbol{u}_h - \widehat{\boldsymbol{u}}_h), \delta(P_M \boldsymbol{u}_h - \widehat{\boldsymbol{u}}_h)\rangle_{\partial\mathcal{T}_h} + \langle (\widehat{\underline{\boldsymbol{\sigma}}}_h - \underline{\boldsymbol{\sigma}}_h)\boldsymbol{n}, \delta(\boldsymbol{u}_h - \widehat{\boldsymbol{u}}_h)\rangle_{\partial\mathcal{T}_h}\\
&= (\rho \boldsymbol{v}_h, \delta \boldsymbol{v}_h)_{\mathcal{T}_h} + (\underline{\boldsymbol{\sigma}}_h, \nabla\delta\boldsymbol{u}_h)_{\mathcal{T}_h} - \langle \widehat{\underline{\boldsymbol{\sigma}}}_h\boldsymbol{n}, \delta\boldsymbol{u}_h\rangle_{\partial\mathcal{T}_h} - (\boldsymbol{f}, \delta \boldsymbol{u}_h)_{\mathcal{T}_h}\\
&\quad + \langle \tau(P_M \boldsymbol{u}_h - \widehat{\boldsymbol{u}}_h), \delta(P_M \boldsymbol{u}_h - \widehat{\boldsymbol{u}}_h)\rangle_{\partial\mathcal{T}_h} + \langle (\widehat{\underline{\boldsymbol{\sigma}}}_h - \underline{\boldsymbol{\sigma}}_h)\boldsymbol{n}, \delta(\boldsymbol{u}_h - \widehat{\boldsymbol{u}}_h)\rangle_{\partial\mathcal{T}_h}.
\end{aligned}$$

by equation (15e) with $\boldsymbol{\mu} := \delta\widehat{\boldsymbol{u}}_h$ and since, by equation (15f), $\delta\widehat{\boldsymbol{u}}_h = 0$ on Γ_D. Finally, by definition of P_M, we get

$$\begin{aligned}
\delta H_h^{HDG} = &(\rho \boldsymbol{v}_h, \delta \boldsymbol{v}_h)_{\mathcal{T}_h} + (\underline{\boldsymbol{\sigma}}_h, \nabla\delta\boldsymbol{u}_h)_{\mathcal{T}_h} - \langle \widehat{\underline{\boldsymbol{\sigma}}}_h\boldsymbol{n}, \delta\boldsymbol{u}_h\rangle_{\partial\mathcal{T}_h} - (\boldsymbol{f}, \delta \boldsymbol{u}_h)_{\mathcal{T}_h}\\
&+ \langle (\widehat{\underline{\boldsymbol{\sigma}}}_h - \underline{\boldsymbol{\sigma}}_h)\boldsymbol{n} + \tau(P_M \boldsymbol{u}_h - \widehat{\boldsymbol{u}}_h), \delta(P_M \boldsymbol{u}_h - \widehat{\boldsymbol{u}}_h)\rangle_{\partial\mathcal{T}_h}.
\end{aligned}$$

Note that, until now, we have not used the particular form of the numerical traces. Next, we insert the definition of the HDG numerical trace for the flux, (13), to get

$$\delta H_h^{HDG} =(\rho \boldsymbol{v}_h, \delta \boldsymbol{v}_h)_{\mathcal{T}_h} + (\underline{\boldsymbol{\sigma}}_h, \nabla \delta \boldsymbol{u}_h)_{\mathcal{T}_h} - \langle \widehat{\underline{\boldsymbol{\sigma}}}_h \boldsymbol{n}, \delta \boldsymbol{u}_h\rangle_{\partial\mathcal{T}_h} - (\boldsymbol{f}, \delta \boldsymbol{u}_h)_{\mathcal{T}_h}.$$

Thus, using the definition of the discrete Poisson bracket, we get that

$$\begin{aligned}
(\rho\, \dot{\boldsymbol{u}}_h, \boldsymbol{w})_{\mathcal{T}_h} &= \dot{C}_{\boldsymbol{u}_h}(\boldsymbol{w}) = \{C_{\boldsymbol{u}_h}(\boldsymbol{w}), H_h^{HDG}\}_h = (\frac{\delta H_h^{HDG}}{\delta \boldsymbol{v}_h}, \boldsymbol{w})_{\mathcal{T}_h} = (\boldsymbol{\rho} v_h, \boldsymbol{w})_{\mathcal{T}_h},\\
(\rho\, \dot{\boldsymbol{v}}_h, \boldsymbol{w})_{\mathcal{T}_h} &= \dot{C}_{\boldsymbol{v}_h}(\boldsymbol{w}) = \{C_{\boldsymbol{v}_h}(\boldsymbol{w}), H_h^{HDG}\}_h = (\frac{\delta H_h^{HDG}}{\delta \boldsymbol{u}_h}, \boldsymbol{w})_{\mathcal{T}_h} = (\underline{\boldsymbol{\sigma}}_h, \nabla \boldsymbol{w})_{\mathcal{T}_h}\\
&\qquad - \langle \widehat{\underline{\boldsymbol{\sigma}}}_h \boldsymbol{n}, \boldsymbol{w}\rangle_{\partial\mathcal{T}_h}\\
&\qquad - (\boldsymbol{f}, \boldsymbol{w})_{\mathcal{T}_h},
\end{aligned}$$

for all $\boldsymbol{w} \in \boldsymbol{W}_h$. Therefore, semidiscrete HDG methods defines a Hamiltonian dynamical system. This completes the proof. $\square$

4.1.3. The semidiscrete DG method

Theorem 3 (Hamiltonian structure of the semidiscrete DG methods). *The DG method defined in* (15) *with numerical traces given by* (14) *defines a Hamiltonian dynamical system.*

Proof. The variation of the functional H_h^{DG} is

$$\begin{aligned}
\delta H_h^{DG} =&(\rho \boldsymbol{v}_h, \delta \boldsymbol{v}_h)_{\mathcal{T}_h} + (\mathcal{C}\underline{\boldsymbol{\epsilon}}_h, \delta \underline{\boldsymbol{\epsilon}}_h)_{\mathcal{T}_h} - (\boldsymbol{f}, \delta \boldsymbol{u}_h)_{\mathcal{T}_h} - \langle \boldsymbol{\sigma}_N, \delta \widehat{\boldsymbol{u}}_h\rangle_{\mathcal{F}_h^N}\\
&- C_{11}\langle [\![\boldsymbol{u}_h \otimes \boldsymbol{n}]\!], [\![\delta \boldsymbol{u}_h \otimes \boldsymbol{n}]\!]\rangle_{\mathcal{F}_h^0\cup\mathcal{F}_h^D} - C_{22}\langle [\![\underline{\boldsymbol{\sigma}}_h \boldsymbol{n}]\!], [\![\delta \underline{\boldsymbol{\sigma}}_h \boldsymbol{n}]\!]\rangle_{\mathcal{F}_h^0\cup\mathcal{F}_h^N}
\end{aligned}$$

Proceeding as in the previous proof, we get

$$\delta H_h^{DG} =(\rho \boldsymbol{v}_h, \delta \boldsymbol{v}_h)_{\mathcal{T}_h} + (\underline{\boldsymbol{\sigma}}_h, \nabla \delta \boldsymbol{u}_h)_{\mathcal{T}_h} - \langle \widehat{\underline{\boldsymbol{\sigma}}}_h \boldsymbol{n}, \delta \boldsymbol{u}_h\rangle_{\partial\mathcal{T}_h} - (\boldsymbol{f}, \delta \boldsymbol{u}_h)_{\mathcal{T}_h} + \Theta_h,$$

where

$$\begin{aligned}
\Theta_h :=&\Phi_h - C_{11}\langle [\![\boldsymbol{u}_h \otimes \boldsymbol{n}]\!], [\![\delta \boldsymbol{u}_h \otimes \boldsymbol{n}]\!]\rangle_{\mathcal{F}_h^0\cup\mathcal{F}_h^D} - C_{22}\langle [\![\underline{\boldsymbol{\sigma}}_h \boldsymbol{n}]\!], [\![\delta \underline{\boldsymbol{\sigma}}_h \boldsymbol{n}]\!]\rangle_{\mathcal{F}_h^0\cup\mathcal{F}_h^N},\\
\Phi_h :=&\langle \delta(\boldsymbol{u}_h - \widehat{\boldsymbol{u}}_h), (\widehat{\underline{\boldsymbol{\sigma}}}_h - \underline{\boldsymbol{\sigma}}_h)\boldsymbol{n}\rangle_{\partial\mathcal{T}_h}.
\end{aligned}$$

We claim that, if we insert the definition of the numerical traces, (14), we get that $\Theta_h = 0$. In this case, we then obtain

$$\delta H_h^{DG} = (\rho \boldsymbol{v}_h, \delta \boldsymbol{v}_h)_{\mathcal{T}_h} + (\underline{\boldsymbol{\sigma}}_h, \nabla \delta \boldsymbol{u}_h)_{\mathcal{T}_h} - \langle \widehat{\underline{\boldsymbol{\sigma}}}_h \boldsymbol{n}, \delta \boldsymbol{u}_h\rangle_{\partial\mathcal{T}_h} - (\boldsymbol{f}, \delta \boldsymbol{u}_h)_{\mathcal{T}_h},$$

and we proceed exactly as in the proof of the semidiscrete HDG method to conclude that the semidiscrete DG method defines a Hamiltonian system.

It remains to prove the claim. By Lemma Appendix A.1 with $\boldsymbol{w} := \delta(\boldsymbol{u}_h - \widehat{\boldsymbol{u}}_h)$ and $\underline{\boldsymbol{\chi}} := (\widehat{\underline{\boldsymbol{\sigma}}}_h - \underline{\boldsymbol{\sigma}}_h)$, we have that

$$
\begin{aligned}
\Phi_h =& \langle \{\!\{ \delta(\boldsymbol{u}_h - \widehat{\boldsymbol{u}}_h) \}\!\}, \llbracket (\widehat{\underline{\boldsymbol{\sigma}}}_h - \underline{\boldsymbol{\sigma}}_h)\boldsymbol{n} \rrbracket \rangle_{\mathcal{F}_h^0} \\
&+ \langle \llbracket \delta(\boldsymbol{u}_h - \widehat{\boldsymbol{u}}_h) \otimes \boldsymbol{n} \rrbracket, \{\!\{ (\widehat{\underline{\boldsymbol{\sigma}}}_h - \underline{\boldsymbol{\sigma}}_h) \}\!\} \rangle_{\mathcal{F}_h^0} \\
&+ \langle \delta(\boldsymbol{u}_h - \widehat{\boldsymbol{u}}_h), (\widehat{\underline{\boldsymbol{\sigma}}}_h - \underline{\boldsymbol{\sigma}}_h)\boldsymbol{n} \rangle_{\mathcal{F}_h^D \cup \mathcal{F}_h^N}. \\
=& - \langle \delta(\{\!\{ \boldsymbol{u}_h \}\!\} - \widehat{\boldsymbol{u}}_h), \llbracket \underline{\boldsymbol{\sigma}}_h \boldsymbol{n} \rrbracket \rangle_{\mathcal{F}_h^0} \\
&+ \langle \delta(\llbracket \boldsymbol{u}_h \rrbracket \otimes \boldsymbol{n}, (\widehat{\underline{\boldsymbol{\sigma}}}_h - \{\!\{ \underline{\boldsymbol{\sigma}}_h) \}\!\} \rangle_{\mathcal{F}_h^0} \\
&+ \langle \delta(\boldsymbol{u}_h - \widehat{\boldsymbol{u}}_h), (\widehat{\underline{\boldsymbol{\sigma}}}_h - \underline{\boldsymbol{\sigma}}_h)\boldsymbol{n} \rangle_{\mathcal{F}_h^D \cup \mathcal{F}_h^N},
\end{aligned}
$$

since the numerical traces are single-valued. Inserting the definition of the numerical traces (14), we get

$$
\begin{aligned}
\Phi_h =& \langle \delta(\llbracket \boldsymbol{u}_h \otimes \boldsymbol{n} \rrbracket \cdot \boldsymbol{C}_{12} + C_{22} \llbracket \underline{\boldsymbol{\sigma}}_h \boldsymbol{n} \rrbracket), \llbracket \underline{\boldsymbol{\sigma}}_h \boldsymbol{n} \rrbracket \rangle_{\mathcal{F}_h^0} \\
&+ \langle \delta \llbracket \boldsymbol{u}_h \otimes \boldsymbol{n} \rrbracket, C_{11} \llbracket \boldsymbol{u}_h \otimes \boldsymbol{n} \rrbracket - \llbracket \underline{\boldsymbol{\sigma}}_h \boldsymbol{n} \rrbracket \otimes \boldsymbol{C}_{12} \rangle_{\mathcal{F}_h^0} \\
&+ \langle \delta \llbracket \boldsymbol{u}_h \otimes \boldsymbol{n} \rrbracket, C_{11} \llbracket \boldsymbol{u}_h \otimes \boldsymbol{n} \rrbracket \rangle_{\mathcal{F}_h^D} + \langle C_{22} \delta \llbracket \underline{\boldsymbol{\sigma}}_h \boldsymbol{n} \rrbracket, \llbracket \underline{\boldsymbol{\sigma}}_h \boldsymbol{n} \rrbracket \rangle_{\mathcal{F}_h^N},
\end{aligned}
$$

and the result follows. This proves the claim and completes the proof. □

4.2. The canonical approach

Here, we consider the semidiscrete schemes under consideration as defining a finite dimensional system of ODEs and show that it has the form of a canonical Hamiltonian dynamical system.

We begin by considering a basis of $\boldsymbol{W}_h$, $\{\boldsymbol{\phi}_i\}_{i\in\mathcal{J}}$, such that $(\rho\boldsymbol{\phi}_i, \boldsymbol{\phi}_j)_{\mathcal{T}_h} = \delta_{i,j}$ for $i, j \in \mathcal{J} = \{1, \cdots, \dim \boldsymbol{W}_h\}$. Then, we define the coefficients $u_i(t)$ and $v_i(t)$ associated to the basis $\{\boldsymbol{\phi}_i\}_{i\in\mathcal{J}}$ of the approximations to the displacement $\boldsymbol{u}_h$ and the velocity $\boldsymbol{v}_h$, respectively, that is,

$$
\boldsymbol{u}_h(t, \boldsymbol{x}) = \sum_{i\in\mathcal{J}} u_i(t)\boldsymbol{\phi}_i(\boldsymbol{x}), \qquad \boldsymbol{v}_h(t, \boldsymbol{x}) = \sum_{i\in\mathcal{J}} v_i(t)\boldsymbol{\phi}_i(\boldsymbol{x}). \tag{18}
$$

The canonical coordinates are $(\mathsf{q}_i, \mathsf{p}_i) := (u_i, v_i)$ for $i \in \mathcal{J}$. They are nothing but the degrees of freedom of the approximate solution $(\boldsymbol{u}_h, \boldsymbol{v}_h)$, and coincide with the coordinates functionals of the modern approach because we have that $(\mathsf{q}_i, \mathsf{p}_i) = (C_{\boldsymbol{u}_h}(\phi_i), C_{\boldsymbol{v}_h}(\phi_i))$. This justifies calling the functionals $C_{\boldsymbol{u}_h}(\phi_i)$ and $C_{\boldsymbol{v}_h}(\phi_i)$ the *coordinates* functionals.

Theorem 4 (Canonical Hamiltonian structure of the semidiscrete methods). *The canonical Hamiltonian system:*

$$
\dot{\mathsf{p}}_i = -\frac{\partial}{\partial \mathsf{q}_i}\mathcal{H}(\mathsf{p}, \mathsf{q}), \quad \dot{\mathsf{q}}_i = \frac{\partial}{\partial \mathsf{p}_i}\mathcal{H}(\mathsf{p}, \mathsf{q}) \quad i \in \mathcal{J},
$$

holds for

$$
\begin{aligned}
&\mathcal{H}(\mathsf{p},\mathsf{q}) := H_h^{M}(\boldsymbol{u}_h,\boldsymbol{v}_h), &&(\boldsymbol{u}_h,\boldsymbol{v}_h)\ \textit{solution of the semidiscrete mixed scheme,}\\
&\mathcal{H}(\mathsf{p},\mathsf{q}) := H_h^{HDG}(\boldsymbol{u}_h,\boldsymbol{v}_h), &&(\boldsymbol{u}_h,\boldsymbol{v}_h)\ \textit{solution of the semidiscrete DG scheme,}\\
&\mathcal{H}(\mathsf{p},\mathsf{q}) := H_h^{DG}(\boldsymbol{u}_h,\boldsymbol{v}_h), &&(\boldsymbol{u}_h,\boldsymbol{v}_h)\ \textit{solution of the semidiscrete HDG scheme.}
\end{aligned}
$$

Proof. Since, for $\mathcal{H}(\mathsf{p}_i,\mathsf{q}_i) := H_h(\boldsymbol{u}_h,\boldsymbol{v}_h)$, we have

$$
\begin{aligned}
\frac{\partial}{\partial \mathsf{q}_i}\mathcal{H}_h(\mathsf{p}_i,\mathsf{q}_i) &= \frac{\partial}{\partial \mathsf{q}_i} H_h(\boldsymbol{u}_h,\boldsymbol{v}_h) = \frac{d}{d\eta} H(\boldsymbol{u}_h+\eta\boldsymbol{\phi}_i,\boldsymbol{v}_h)|_{\eta=0} = (\boldsymbol{\phi}_i, \frac{\delta H_h}{\delta \boldsymbol{u}_h})_{\mathcal{T}_h},\\
\frac{\partial}{\partial \mathsf{p}_i}\mathcal{H}_h(\mathsf{p}_i,\mathsf{q}_i) &= \frac{\partial}{\partial \mathsf{p}_i} H_h(\boldsymbol{u}_h,\boldsymbol{v}_h) = \frac{d}{d\eta} H_h(\boldsymbol{u}_h,\boldsymbol{v}_h+\eta\boldsymbol{\phi}_i)|_{\eta=0} = (\boldsymbol{\phi}_i, \frac{\delta H_h}{\delta \boldsymbol{v}_h})_{\mathcal{T}_h},
\end{aligned}
$$

we get, for each of the three Hamiltonians H_h under consideration, by the Theorems 1, 2 and 3, respectively, that

$$
\begin{aligned}
\dot{\mathsf{p}}_i &= \dot{C}_{\boldsymbol{u}_h}(\boldsymbol{\phi}_i) = \{C_{\boldsymbol{u}_h}(\boldsymbol{\phi}_i), H_h\}_h = -(\boldsymbol{\phi}_i, \frac{\delta H_h}{\delta \boldsymbol{v}_h})_{\mathcal{T}_h} = -\frac{\partial}{\partial \mathsf{q}_i}\mathcal{H}(\mathsf{p},\mathsf{q}),\\
\dot{\mathsf{q}}_i &= \dot{C}_{\boldsymbol{v}_h}(\boldsymbol{\phi}_i) = \{C_{\boldsymbol{v}_h}(\boldsymbol{\phi}_i), H_h\}_h = \ (\boldsymbol{\phi}_i, \frac{\delta H_h}{\delta \boldsymbol{u}_h})_{\mathcal{T}_h} = \ \frac{\partial}{\partial \mathsf{p}_i}\mathcal{H}(\mathsf{p},\mathsf{q}).
\end{aligned}
$$

This completes the proof. $\square$

4.3. Conservation properties of the semidiscrete schemes

In this section, we prove a discrete version of the conservation properties of Proposition 2.1.

Proposition 4.1. *Let $(\boldsymbol{u}_h,\boldsymbol{v}_h)$ be any solution of the semidiscrete schemes under consideration. Then the total linear momentum $\boldsymbol{I}(\boldsymbol{v}_h) = \int_\Omega \rho\,\boldsymbol{v}_h$, the total angular momentum $\boldsymbol{J}(\boldsymbol{v}_h) = \int_\Omega \boldsymbol{x}\times\rho\,\boldsymbol{v}_h$, and the total energy*

$$
E(\boldsymbol{u}_h,\boldsymbol{v}_h) = \begin{cases}
\frac12\left((\rho\boldsymbol{v}_h,\boldsymbol{v}_h)_{\mathcal{T}_h} + (\mathcal{A}\,\boldsymbol{\sigma}_h,\boldsymbol{\sigma}_h)_{\mathcal{T}_h}\right), & \textit{mixed method,}\\
\frac12\left((\rho\boldsymbol{v}_h,\boldsymbol{v}_h)_{\mathcal{T}_h} + (\ \mathcal{C}\ \underline{\boldsymbol{\epsilon}}_h, \underline{\boldsymbol{\epsilon}}_h\ )_{\mathcal{T}_h}\right) & \\
\quad +\frac12\langle \tau(P_{\boldsymbol{M}}\boldsymbol{u}_h - \widehat{\boldsymbol{u}}_h), P_{\boldsymbol{M}}\boldsymbol{u}_h - \widehat{\boldsymbol{u}}_h\rangle_{\partial\mathcal{T}_h}, & \textit{HDG method,}\\
\frac12\left((\rho\boldsymbol{v}_h,\boldsymbol{v}_h)_{\mathcal{T}_h} + (\ \mathcal{C}\ \underline{\boldsymbol{\epsilon}}_h, \underline{\boldsymbol{\epsilon}}_h\ )_{\mathcal{T}_h}\right) & \\
\quad -\frac12 C_{11}\langle [\![\boldsymbol{u}_h\otimes\boldsymbol{n}]\!], [\![\boldsymbol{u}_h\otimes\boldsymbol{n}]\!]\rangle_{\mathcal{F}_h^0\cup\mathcal{F}_h^D} & \\
\quad -\frac12 C_{22}\langle [\![\underline{\boldsymbol{\sigma}}_h\boldsymbol{n}]\!], [\![\underline{\boldsymbol{\sigma}}_h\boldsymbol{n}]\!]\rangle_{\mathcal{F}_h^0\cup\mathcal{F}_h^N} & \textit{DG method,}
\end{cases}
$$

are constant in time whenever $\Gamma_D = \emptyset$, and $\boldsymbol{f}$ and $\boldsymbol{\sigma}_N$ are zero. For this to happen for the total angular momentum, the space $\boldsymbol{W}_h$ must include the functions $\boldsymbol{x}\times\boldsymbol{a}$ for every constant vector $\boldsymbol{a}\in\mathbb{R}^3$.

The proof is identical to the proof of the conservation laws for the exact case, Proposition 2.1. It is based on the fact that, if $J = J(\boldsymbol{u}_h(t),\boldsymbol{v}_h(t))$ is a functional defined on the orbits $t\mapsto(\boldsymbol{u}_h(t),\boldsymbol{v}_h(t))$ of a Hamiltonian dynamical system, then $\dot{J} = \{J, H_h\}_h$, where H_h is the Hamiltonian. This holds for the three semidiscrete schemes we are considering by Theorems 1, 2 and 3.

5. Symplectic Hamiltonian finite element methods: Fully discrete schemes

In this section, we discuss the properties we want our symplectic time-marching scheme to have, and argue that the Explicit Symplectic Partitioned Runge-Kutta (ESPRK) methods fulfill them. We then give two examples of fully discrete schemes, one for the semidiscrete HDG method and the other for the Local Discontinuous Galerkin method.

5.1. Properties of the symplectic methods

Let us briefly discuss the three properties we want the symplectic time marching methods to have.

The first concerns the invariants of the Hamiltonian dynamical system. We know that, when $\Gamma_D = \emptyset$, and $\boldsymbol{f}$ and $\boldsymbol{\sigma}_N$ are zero, the linear and angular momenta remain constant. In other words, the linear and angular momenta are linear invariants of the Hamiltonian system defined by the semidiscrete method. Moreover, when the data $\boldsymbol{u}_D$, $\boldsymbol{f}$ and $\boldsymbol{\sigma}_N$ are independent of time, the Hamiltonian is also constant. In other words, the Hamiltonian is a (separable) quadratic invariant of the Hamiltonian system. This implies that, when picking a symplectic time-marching scheme, we want to ensure that it maintains constant linear invariants and quadratic invariants of the original Hamiltonian system. The second property concerns the accuracy of the methods. Since we are using high-order accurate finite elements to discretize in space, the time-marching methods must match their high-order accuracy. The third property is about implementation. Since explicit schemes are very easy to code, and quite efficient for hyperbolic problems, we are interested in choosing explicit time-marching schemes.

The so-called explicit symplectic partitioned Runge-Kutta (ESPRK) methods we use in our numerical experiments, see Appendix C, satisfy all of the above properties except the conservation of quadratic invariants. However, the methods approximate the Hamiltonian without drift in time. We will observe in our computational experiments in Section 6.2 that these oscillations are minute, in theory of order Δt^{k+2}. Hence, it pays to sacrifice exact conservation for efficiency in the implementation.

5.2. Explicit Symplectic Partitioned Runge-Kutta methods (ESPRK)

Let us now define the ESPRK methods for the Hamiltonian system

$$\dot{\mathsf{p}} = -\frac{\partial \mathcal{H}}{\partial \mathsf{q}}(\mathsf{p}, \mathsf{q}, t), \quad \dot{\mathsf{q}} = \frac{\partial \mathcal{H}}{\partial \mathsf{p}}(\mathsf{p}, \mathsf{q}, t).$$

We consider ESPRK methods for the general case of Hamiltonians which depend on time. In our setting, this corresponds to the case in which the data $\boldsymbol{u}_D$, $\boldsymbol{f}$ and $\boldsymbol{\sigma}_N$ depend on time.

So, we define an step $(\mathsf{p}^n, \mathsf{q}^n) \to (\mathsf{p}^{n+1}, \mathsf{q}^{n+1})$ of an s-stages partitioned Runge-Kutta method with coefficients (a_{ij}, b_i, c_i) and $(\tilde{a}_{ij}, \tilde{b}_i, \tilde{c}_i)$, for $i, j = 1, \ldots, s$ by

$$\begin{aligned} \mathsf{p}^{n+1} &= \mathsf{p}^n + \sum_{i=1}^{s} b_i k_i, & \mathsf{q}^{n+1} &= \mathsf{q}^n + \sum_{i=1}^{s} \tilde{b}_i \tilde{k}_i \\ k_i &= -\frac{\partial \mathcal{H}}{\partial \mathsf{q}}(\mathsf{p}^{n,i}, \mathsf{q}^{n,i}, t^n + c_i \Delta t^n), & \tilde{k}_i &= \frac{\partial \mathcal{H}}{\partial \mathsf{p}}(\mathsf{p}^{n,i}, \mathsf{q}^{n,i}, t^n + \tilde{c}_i \Delta t^n), \\ \mathsf{p}^{n,i} &= \mathsf{p}^n + \Delta t^n \sum_{j=1}^{s} a_{ij} k_j & \mathsf{q}^{n,i} &= \mathsf{q}^n + \Delta t^n \sum_{j=1}^{s} \tilde{a}_{ij} \tilde{k}_j \end{aligned}$$

In order to define explicit schemes, we consider an explicit and diagonally implicit Runge-Kutta methods of the form

$$a_{ij} = \begin{cases} 0, & \text{if } i < j \\ b_j, & \text{if } i \geq j \end{cases} \qquad \tilde{a}_{ij} = \begin{cases} 0, & \text{if } i \leq j \\ \tilde{b}_j, & \text{if } i > j. \end{cases}$$

For the separable Hamiltonian of elastodynamics, the explicit symplectic partitioned Runge-Kutta scheme reads as follow:

$$\begin{aligned} \mathsf{p}^{n,i} &= \mathsf{p}^n + \sum_{j=1}^{i} b_j k_j, & \mathsf{q}^{n,i} &= \mathsf{q}^n + \sum_{j=1}^{i-1} \tilde{b}_j \tilde{k}_j \\ k_j &= -\frac{\partial \mathcal{H}}{\partial \mathsf{q}}(\mathsf{q}^{n,j}, t^n + c_j \Delta t^n), & \tilde{k}_j &= \frac{\partial \mathcal{H}}{\partial \mathsf{p}}(\mathsf{p}^{n,j}, t^n + \tilde{c}_j \Delta t^n), \end{aligned}$$

for $i = 1, \ldots, s$. The next step is obtained by setting $\mathsf{p}^{n+1} := \mathsf{p}^{n,s}$ and $\mathsf{q}^{n+1} := \mathsf{q}^{n,s}$. See Appendix Appendix C for the Butcher tableau of the ESPRK methods of order of accuracy from 3 to 6 we use in our numerical experiments.

330 *5.3. Fully discrete HDG method*

We consider the HDG semidiscrete scheme (15) with numerical traces given by the numerical traces (13) and spaces $\underline{\boldsymbol{V}}_h$, $\boldsymbol{W}_h$ and $\boldsymbol{M}_h$. We assume that for a given time t^n the values of the variables are known, we denote these by $(\boldsymbol{u}_h^n, \boldsymbol{v}_h^n, \underline{\boldsymbol{\epsilon}}_h^n, \underline{\boldsymbol{\sigma}}_h^n, \widehat{\boldsymbol{u}}_h^n)$, and they correspond to the 0-stage of an ESPRK scheme.
335 Then, the i-stage of the method, for a time step Δt^n is defined by the equations

$$\begin{aligned} (\rho\, \boldsymbol{v}_h^{n,i}, \boldsymbol{w})_K &= (\rho\, \boldsymbol{v}_h^{n,i-1}, \boldsymbol{w})_K + b_i \Delta t^n \big((\underline{\boldsymbol{\sigma}}_h^{n,i-1}, \nabla \boldsymbol{w})_K + \langle \widehat{\underline{\boldsymbol{\sigma}}}_h^{n,i-1} \boldsymbol{n}, \boldsymbol{w} \rangle_{\partial K} \\ &\qquad + (\boldsymbol{f}(t^n + c_i \Delta t^n), \boldsymbol{w})_K \big), \\ (\boldsymbol{u}_h^{n,i}, \boldsymbol{w})_K &= (\boldsymbol{u}_h^{n,i-1}, \boldsymbol{w})_K \quad + \tilde{b}_i \Delta t^n (\boldsymbol{v}_h^{n,i}, \boldsymbol{w})_K, \end{aligned}$$

for all $\boldsymbol{w} \in \boldsymbol{W}(K)$, where the numerical trace of the stress is

$$\widehat{\underline{\boldsymbol{\sigma}}}_h^{n,i-1} = \underline{\boldsymbol{\sigma}}_h^{n,i-1} - \tau(P_M \boldsymbol{u}_h^{n,i-1} - \widehat{\boldsymbol{u}}_h^{n,i-1}) \quad \text{on } \partial K,$$

and $i = 1, \dots, s$. Observe that this procedure will only allow us to advance to the (i)-stage the variables $\boldsymbol{v}_h^{n,i}$ and $\boldsymbol{u}_h^{n,i}$. From the equations above is clear that we also need to obtain at least $\underline{\boldsymbol{\sigma}}_h^{n,i}$ and $\widehat{\underline{\boldsymbol{\sigma}}}_h^{n,i}$. In order to advance the other variables we need to solve the following global system for $(\underline{\boldsymbol{\epsilon}}_h^{n,i}, \underline{\boldsymbol{\sigma}}_h^{n,i}, \widehat{\boldsymbol{u}}_h^{n,i})$, which are obtained from the steady-state part of the scheme (15), namely,

$$
\begin{aligned}
(\underline{\boldsymbol{\epsilon}}_h^{n,i}, \underline{\boldsymbol{\chi}})_{\mathcal{T}_h} - \langle \widehat{\boldsymbol{u}}_h^{n,i}, \underline{\boldsymbol{\chi}}\boldsymbol{n}\rangle_{\partial\mathcal{T}_h\setminus\Gamma_D} &= -(\boldsymbol{u}_h^{n,i}, \nabla\cdot\underline{\boldsymbol{\chi}})_{\mathcal{T}_h} + \langle \widehat{\boldsymbol{u}}_D(t^n + c_i\Delta t^n)), \underline{\boldsymbol{\chi}}\boldsymbol{n}\rangle_{\Gamma_D},\\
(\underline{\boldsymbol{\sigma}}_h^{n,i}, \underline{\boldsymbol{\chi}})_{\mathcal{T}_h} - (\mathcal{C}\underline{\boldsymbol{\epsilon}}_h^{n,i}, \underline{\boldsymbol{\chi}})_{\mathcal{T}_h} &= 0,\\
\langle \widehat{\underline{\boldsymbol{\sigma}}}_h^{n,i}, \boldsymbol{\mu}\rangle_{\partial\mathcal{T}_h\setminus\Gamma_D} &= \langle \boldsymbol{\sigma}_N(t^n + c_i\Delta t^n), \boldsymbol{\mu}\rangle_{\Gamma},
\end{aligned}
$$

for all $\underline{\boldsymbol{\chi}} \in \underline{\boldsymbol{V}}_h$, and $\boldsymbol{\mu} \in \boldsymbol{M}_h$. The solution of this system exists and is unique, and can be easily computed, as we argue in Appendix Appendix B.

5.4. Fully discrete local discontinuous Galerkin (LDG) method

We consider the DG semidiscrete scheme in (15) and DG fluxes defined in (14). We set $C_{22} = 0$, that is, we consider a local discontinuous Galerkin method. We assume that for a given time t^n the values of the variables are known, we denote these by $(\boldsymbol{u}_h^n, \boldsymbol{v}_h^n, \underline{\boldsymbol{\epsilon}}_h^n, \underline{\boldsymbol{\sigma}}_h^n)$, and they correspond to the 0-stage of the ESPRK algorithm. Then, the i-stage of the method, for a time step Δt^n is defined by the local equations

$$
\begin{aligned}
(\rho\, \boldsymbol{v}_h^{n,i}, \boldsymbol{w})_K &= (\rho\, \boldsymbol{v}_h^{n,i-1}, \boldsymbol{w})_K + b_i\Delta t^n\big((\underline{\boldsymbol{\sigma}}_h^{n,i-1}, \nabla\boldsymbol{w})_K + \langle \widehat{\underline{\boldsymbol{\sigma}}}_h^{n,i-1}\boldsymbol{n}, \boldsymbol{w}\rangle_{\partial K},\\
&\qquad + (\boldsymbol{f}(t^n + c_i\Delta t^n), \boldsymbol{w})_K\big),\\
(\boldsymbol{u}_h^{n,i}, \boldsymbol{w})_K &= (\boldsymbol{u}_h^{n,i-1}, \boldsymbol{w})_K + \tilde{b}_i\Delta t^n(\boldsymbol{v}_h^{n,i}, \boldsymbol{w})_K,
\end{aligned}
$$

for $i = 1, \dots, s$ and for all $\boldsymbol{w} \in \boldsymbol{W}_h$ and numerical trace

$$
\widehat{\underline{\boldsymbol{\sigma}}}_h^{n.i-1} = \begin{cases}
\{\!\{\underline{\boldsymbol{\sigma}}_h^{n,i-1}\}\!\} + C_{11}[\![\boldsymbol{u}_h^{n,i-1}\otimes\boldsymbol{n}]\!] - [\![\underline{\boldsymbol{\sigma}}_h^{n,i-1}\boldsymbol{n}]\!]\otimes\boldsymbol{C}_{12}, & \text{if } F \in \mathcal{F}_h^0\\
\underline{\boldsymbol{\sigma}}_h^{n,i-1} + C_{11}[\![\boldsymbol{u}_h^{n,i-1}\otimes\boldsymbol{n}]\!], & \text{if } F \in \mathcal{F}_h^D\\
\boldsymbol{\sigma}_N(t^n + c_{i-1}\Delta t^n), & \text{if } F \in \mathcal{F}_h^N.
\end{cases}
$$

As in the previous case, in order to advance to the next stage is necessary to compute $\underline{\boldsymbol{\sigma}}_h^{n,i}$ (the numerical trace $\widehat{\underline{\boldsymbol{\sigma}}}_h^{n,i}$ is obtained from $\boldsymbol{u}_h^{n,i}$ and $\underline{\boldsymbol{\sigma}}_h^{n,i}$). To do that, we solve the local system

$$
\begin{aligned}
(\underline{\boldsymbol{\epsilon}}_h^{n,i}, \underline{\boldsymbol{\chi}})_K &= \langle \widehat{\boldsymbol{u}}_h^{n,i}, \underline{\boldsymbol{\chi}}\boldsymbol{n}\rangle_{\partial K} - (\boldsymbol{u}_h^{n,i}, \nabla\cdot\underline{\boldsymbol{\chi}})_K,\\
(\underline{\boldsymbol{\sigma}}_h^{n,i}, \underline{\boldsymbol{\chi}})_K &= (\mathcal{C}\underline{\boldsymbol{\epsilon}}_h^{n,i}, \underline{\boldsymbol{\chi}})_K,
\end{aligned}
$$

for all $\underline{\boldsymbol{\chi}} \in \underline{\boldsymbol{V}}(K)$, where

$$
\widehat{\boldsymbol{u}}_h^{n,i} = \begin{cases}
\{\!\{\boldsymbol{u}_h^{n,i}\}\!\} + [\![\boldsymbol{u}_h^{n,i}\otimes\boldsymbol{n}]\!]\boldsymbol{C}_{12}, & \text{if } F \in \mathcal{F}_h^0,\\
\boldsymbol{u}_D(t^n + c_i\Delta t^n) & \text{if } F \in \mathcal{F}_h^D,\\
\boldsymbol{u}_h^{n,i} & \text{if } F \in \mathcal{F}_h^N.
\end{cases}
$$

Therefore, we obtain a fully discrete DG scheme, which is explicit in time and local in space.

6. Numerical experiments

In this section, we test the properties of the ESPRK(k+2)-HDG$_k$+ numerical scheme introduced in Section 5.3. We use an ESPRK method of order $(k+2)$ when polynomials of degree k are used in the HDG$_k$+ method. In this way, we match the expected rate of convergence of the error of the displacement variable. We consider isotropic materials with stiffness tensor $\mathcal{C}\underline{\boldsymbol{\epsilon}} = 2\mu\boldsymbol{\epsilon} + \lambda \operatorname{tr}(\boldsymbol{\epsilon})\, \boldsymbol{I}$, where λ and μ are the Lamé constants. In Section 6.1, we provide numerical evidence of the approximation properties of the numerical methods showing the optimal convergence of order $k+2$ for the L^2-errors of the displacement and velocity variables and of order $k+1$ for the L^2-errors of the stress and strain variables. In Section 6.2, we present numerical examples illustrating the energy-conserving property of our method.

6.1. History of convergence tests

In the following numerical experiments, we provide evidence of the optimal approximation properties of the numerical scheme ESPRK($k+2$)-HDG$_k$+. For each of the approximations $\boldsymbol{u}_h$, $\boldsymbol{v}_h$, $\underline{\boldsymbol{\epsilon}_h}$ and $\underline{\boldsymbol{\sigma}_h}$, we compute the maximum over the time steps t^n of the L^2-errors of the corresponding error, and then estimate their orders of convergence (e.o.c.). For instance, for the displacement approximation we compute

$$\mathrm{error}_h = \max_{t^n} \|\boldsymbol{u}(t^n) - \boldsymbol{u}_h^n\|_{L^2(\Omega)^2}, \qquad \mathrm{e.o.c}_h = \frac{\log(\mathrm{error}_h/\mathrm{error}_{h'})}{\log(h/h')},$$

where h' correspond to the previous mesh size parameter used in the computations. The experiments are carried on the unit square domain $\Omega = (0,1)^2$ using uniform triangulations with mesh-size parameter $h = 2^{-l}$. As exact solution we take

$$\boldsymbol{u}(x,y,t) = \begin{pmatrix} -x^2y(2y-1)(x-1)^2(y-1)\sin(\pi t) \\ y^2x(2x-1)(y-1)^2(x-1)\sin(\pi t) \end{pmatrix}.$$

We approximate the linear elastodynamics Dirichlet problem, i.e. $\Gamma_D = \partial\Omega$ and $\Gamma_N = \emptyset$, with homogeneous boundary condition $\boldsymbol{u}_D = \boldsymbol{0}$, and data $\boldsymbol{f}$ and initial conditions $\boldsymbol{u}_0$ and $\boldsymbol{v}_0$ so that the equation (1a) and initial (1c) are satisfied. We compute up to final time $T = 0.5$.

We consider two tests on homogeneous media $\rho = 1$, compressible and nearly incompressible materials.

a) Compressible case

We use as material parameters Young's modulus $E = 2.5$ and Poisson ratio $\nu = .25$, equivalently Lamé constants $\lambda = 1$, $\mu = 1$. We summarize the results in Table 1. We observe optimal convergence of order $k+2$ for the approximation error of the displacement and velocity variables and optimal convergence of order $k+1$ for the approximation error of the strain and stress variables.

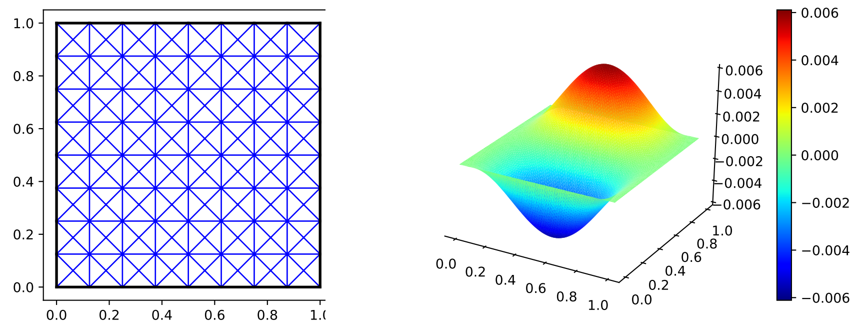

Figure 1: Left: uniform crisscross triangulation ($l = 3$) used in our computations. Right: approximate solution $(\boldsymbol{u}_h)_1$ for $k = 1$ and $l = 4$. Numerical example in Section 6.1 a) Compressible case.

Table 1: History of convergence of the numerical approximations of the linear elastodynamics equations by the scheme ESPRK($k+2$)-HDG$_k$+. Computations were performed up to a final time $T = 0.5$. Compressible case $E = 2.5$ and $\nu = .25$.

		u_h		v_h		$\boldsymbol{\sigma}_h$		$\boldsymbol{\epsilon}_h$	
k	l	error	e.o.c.	error	e.o.c.	error	e.o.c.	error	e.o.c.
1	0	3.4e-3	–	1.1e-2	–	2.0e-2	–	8.3e-3	–
	1	5.5e-4	2.61	2.4e-3	2.19	7.1e-3	1.47	2.9e-3	1.51
	2	6.6e-5	3.05	3.5e-4	2.78	2.1e-3	1.77	8.6e-4	1.76
	3	8.3e-6	3.00	4.6e-5	2.93	5.4e-4	1.94	2.2e-4	1.95
	4	1.0e-6	3.02	5.9e-6	2.98	1.4e-4	1.98	5.7e-5	1.98
2	0	1.1e-3	–	3.7e-3	–	6.6e-3	–	2.8e-3	–
	1	7.6e-5	3.91	3.8e-4	3.28	1.6e-3	2.02	6.8e-4	2.04
	2	4.8e-6	3.99	2.7e-5	3.83	2.3e-4	2.83	9.5e-5	2.84
	3	2.9e-7	4.05	1.7e-6	4.00	2.9e-5	2.97	1.2e-5	2.98
	4	1.8e-8	4.02	1.0e-7	4.00	3.7e-6	2.98	1.5e-6	2.99
3	0	3.4e-4	–	1.1e-3	–	2.8e-3	–	1.2e-3	–
	1	1.2e-5	4.84	6.7e-5	4.11	2.6e-4	3.42	1.1e-4	3.43
	2	3.6e-7	5.03	2.0e-6	5.03	1.7e-5	3.97	6.9e-6	3.98
	3	1.1e-8	5.06	6.3e-8	5.02	1.0e-6	4.00	4.3e-7	4.00
	4	3.4e-10	5.02	2.0e-9	5.01	6.5e-8	3.99	2.7e-8	3.99
4	0	1.1e-4	–	3.9e-4	–	8.2e-4	–	3.5e-4	–
	1	1.0e-6	6.75	5.9e-6	6.04	2.2e-5	5.21	9.3e-6	5.22
	2	1.6e-8	5.97	9.1e-8	6.02	6.9e-7	5.01	2.9e-7	5.02
	3	2.4e-10	6.07	1.4e-9	6.00	2.1e-8	5.01	9.0e-9	5.01
	4	3.7e-12	6.02	2.2e-11	6.00	6.7e-10	5.00	2.8e-10	5.00

b) Near incompressible case

We use as material parameters Young's modulus $E = 3002/1001$ and Poisson ratio $\nu = 500/1001$, equivalently Lamé constants $\lambda = 1000$, $\mu = 1$. We summarize the results in Table 2. We observe optimal convergence of order $k+2$ for the approximation error of the displacement and velocity variables and optimal convergence of order $k+1$ for the approximation error of the strain and stress variables.

Table 2: History of convergence of the numerical approximations of the linear elastodynamics equations by the scheme ESPRK($k+2$)-HDG$_k$+. Computations were performed up to a final time $T = 0.5$. Near incompressible case $E = 3002/1001$ and $\nu = 500/1001$.

		u_h		v_h		$\boldsymbol{\sigma}_h$		$\boldsymbol{\epsilon}_h$	
k	l	error	e.o.c.	error	e.o.c.	error	e.o.c.	error	e.o.c.
1	0	5.4e-03	–	2.0e-02	–	1.4e-02	–	3.7e-02	–
	1	1.1e-03	2.28	4.2e-03	2.27	3.7e-03	2.14	8.5e-03	1.92
	2	1.6e-04	2.82	8.2e-04	2.37	1.8e-03	0.95	4.4e-03	1.06
	3	2.0e-05	3.01	9.7e-05	3.07	4.8e-04	1.87	1.2e-03	1.88
	4	2.4e-06	3.04	1.2e-05	2.97	1.2e-04	2.00	3.0e-04	2.01
2	0	3.1e-03	–	1.1e-02	–	4.7e-03	–	1.0e-02	–
	1	1.6e-04	4.27	7.4e-04	3.91	1.3e-03	1.62	3.3e-03	1.89
	2	1.2e-05	3.68	6.2e-05	3.57	2.1e-04	2.62	5.3e-04	2.61
	3	7.4e-07	4.06	3.8e-06	4.03	2.6e-05	2.98	6.7e-05	2.98
	4	4.5e-08	4.06	2.4e-07	3.97	3.3e-06	3.00	8.4e-06	3.00
3	0	6.6e-04	–	2.3e-03	–	2.5e-03	–	6.6e-03	–
	1	3.4e-05	4.27	1.7e-04	3.74	2.4e-04	3.41	6.1e-04	3.36
	2	9.9e-07	5.10	5.2e-06	5.00	1.5e-05	4.04	3.7e-05	4.03
	3	3.0e-08	5.07	1.6e-07	5.01	9.3e-07	3.99	2.4e-06	3.99
	4	9.0e-10	5.04	4.6e-09	5.14	5.8e-08	3.99	1.5e-07	3.99
4	0	3.2e-04	–	1.1e-03	–	7.6e-04	–	1.9e-03	–
	1	3.2e-06	6.66	1.7e-05	5.99	2.1e-05	5.12	5.4e-05	5.14
	2	4.5e-08	6.14	2.7e-07	5.97	6.6e-07	5.02	1.7e-06	5.02
	3	7.3e-10	5.96	4.2e-09	6.00	2.1e-08	5.01	5.2e-08	5.01
	4	1.1e-11	6.04	2.7e-11	7.24	6.5e-10	4.99	1.6e-09	4.99

6.2. Conservation properties tests

We present three examples showing the energy-conserving properties of the numerical scheme ESPRK($k+2$)-HDG$_k$+.

a) Plane waves

We consider the exact solution $\boldsymbol{u}(x,y,t) = A\boldsymbol{e}\exp(((x,y)\cdot\boldsymbol{d} - c\,t))$, where A is the amplitude, $\boldsymbol{e}$ displacement direction, $\boldsymbol{d}$ propagation direction, and c propagation speed on the two-dimensional domain $\Omega = (0,3)\times(0,1)$ with periodic boundary conditions. We solve two cases, first $\boldsymbol{e} = \boldsymbol{d} = (0,1)$ (P-wave) and second $\boldsymbol{e} = (1,0)$ and $\boldsymbol{d} = (0,1)$ (S-wave). Computations are performed until final time $T = 100$. We take the following material parameters: $A = .1$, $\rho = 1.0$, $E = 3.0$, $\nu = 0.3$. We also use $h = 6.25\times10^{-2}$, $\Delta t = 7.775\times10^{-3}$, $k = 1$ and $\tau = 1/h$. Mesh deformation plots were performed on a coarser mesh ($2h$) to improve visualization.

In Fig. 2, we plot the resulting deformations of the criss-cross triangulation and the plot of the error of the energy E_h (or, equivalently, in the free body case the Hamiltonian functional H_h^{HDG}), that is,

$$E_h(\boldsymbol{u}_h,\boldsymbol{v}_h) = \frac{1}{2}\left((\rho\,\boldsymbol{v}_h,\boldsymbol{v}_h)_{\mathcal{T}_h} + (\mathcal{C}\,\underline{\boldsymbol{\epsilon}}_h,\underline{\boldsymbol{\epsilon}}_h)_{\mathcal{T}_h} + \langle\tau(P_{\boldsymbol{M}}\boldsymbol{u}_h - \widehat{\boldsymbol{u}}_h), P_{\boldsymbol{M}}\boldsymbol{u}_h - \widehat{\boldsymbol{u}}_h\rangle_{\partial\mathcal{T}_h}\right). \tag{19}$$

We also plot the error of the energy resulting of neglecting the terms on the skeleton, that is,

$$\tilde{E}_h(\boldsymbol{u}_h,\boldsymbol{v}_h) = \frac{1}{2}\left((\rho\,\boldsymbol{v}_h,\boldsymbol{v}_h)_{\mathcal{T}_h} + (\mathcal{C}\,\underline{\boldsymbol{\epsilon}}_h,\underline{\boldsymbol{\epsilon}}_h)_{\mathcal{T}_h}\right). \tag{20}$$

We observe that the error of E_h remains practically constant in time, as expected, by the construction of the method. We also observe that the error of $\tilde{E}_h$ oscillates but seems constant in average.

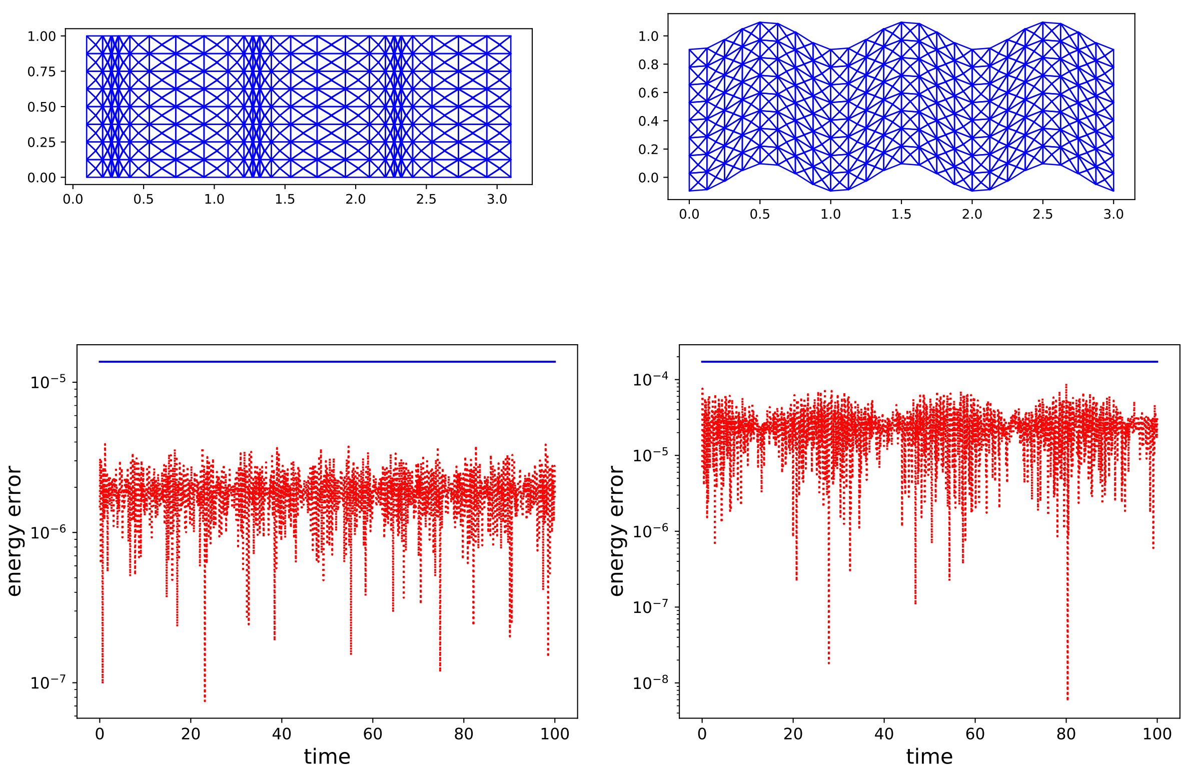

Figure 2: Plot of approximate solution and energy errors of example a) Plane waves. First row: Mesh deformation under plane waves. Left: P-wave ($\boldsymbol{e} = \boldsymbol{d} = (0, 1)$). Right: S-wave ($\boldsymbol{e} = (0, 1)$ and $\boldsymbol{d} = (1, 0)$). Second row: Plots of the errors $|E - E_h|$ (blue straight line) and $|E - \tilde{E}_h|$ (red oscillatory line) of the discrete approximate energies defined in (19) and (20) for the P-wave (left) and S-wave (right).

b) Traveling wave pulse

We consider the exact solution

$$\boldsymbol{u}(x, y, t) = \begin{pmatrix} \phi(x - ct) + \phi(y - ct) \\ 0 \end{pmatrix}, \qquad \phi(s) = (2s - 2)^{10}(2s)^{10}.$$

on the domain $\Omega = (0, 1)^2$ with periodic boundary conditions and material parameters $E = 2.5$ and $\nu = 0.25$. We compute until final time $T = 30$. We take $h = 6.25 \times 10^{-2}$, $\Delta t = 4.511 \times 10^{-3}$, $k = 2$ and $\tau = 1/h$.

In Fig. 3, we plot the first component of the displacement, $(\boldsymbol{u}_h)_1$, and the first component of the velocity, $(\boldsymbol{v}_h)_1$. We also plot the error of the energy E_h and $\tilde{E}_h$ with respect to time. We observe no energy dissipation in time.

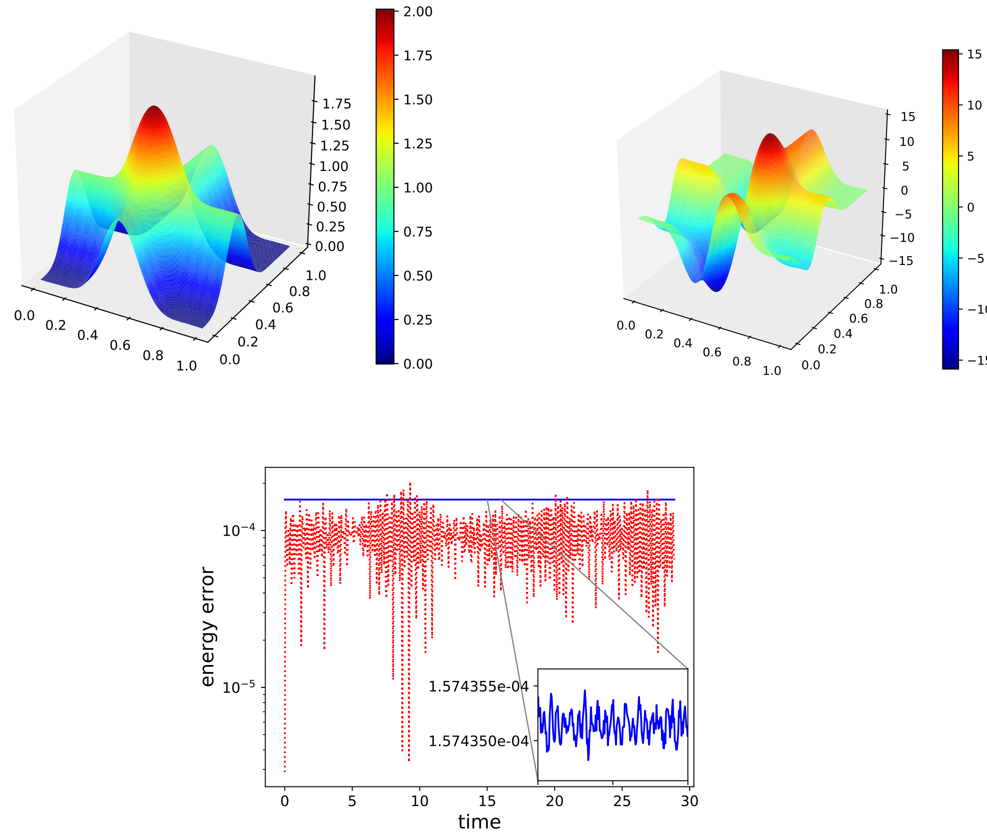

Figure 3: Plot of approximate solution and energy error of example b) Traveling wave pulse. First row: from left to right, approximate solutions $(\boldsymbol{u}_h)_1$ and $(\boldsymbol{v}_h)_1$. Second row: the errors $|E - E_h|$ (blue straight line) and $|E - \tilde{E}_h|$ (red oscillatory line) of the discrete approximate energies defined in (19) and (20), respectively. The zoom of the blue line indicates that the approximate energy E_h is not maintained constant by the ESPRK(3) method, as expected. However, it clearly stays oscillating around a constant, as a consequence of the symplecticity of the method ESPRK(3). Moreover, the oscillations of the blue line are of the size of 5×10^{-10}. So, for all practical purposes, the energy E_h remains essentially constant.

c) Plane stress cantilever beam

We consider the two dimensional domain $\Omega = (0, 1) \times (0, 0.05)$. We consider the linear elastodynamics problem with $\boldsymbol{f} = \boldsymbol{0}$, boundary conditions

$$\boldsymbol{u} = \boldsymbol{0} \quad \text{at } x = 0, \quad \underline{\boldsymbol{\sigma}} \cdot \boldsymbol{n} = \boldsymbol{0} \quad \text{at } y = 0,\, y = 0.05, \text{ at } x = 1,$$

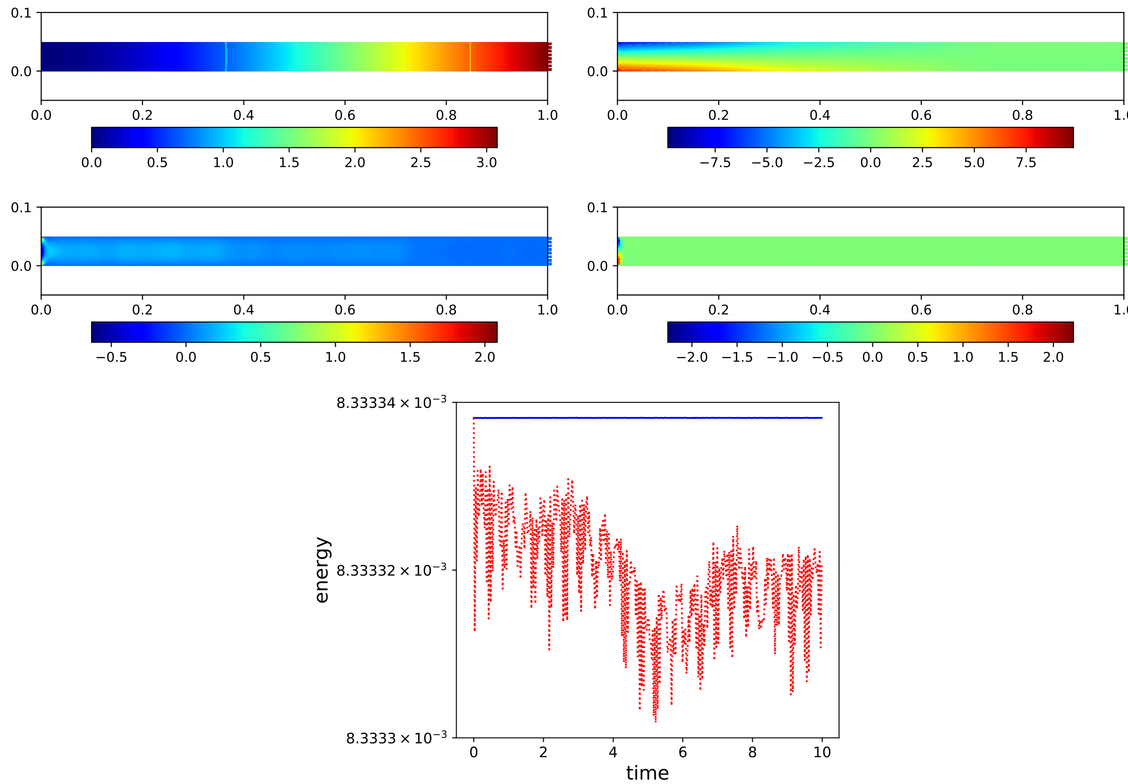

Figure 4: Plot of approximate solution and energy error of example c) Plane stress cantilever beam at final time $T = 10$. First row: Plot of the approximations $(u_h)_2$ (left) and $(\underline{\sigma}_h)_{11}$ (right). Second row: Plot of the approximations $(\underline{\sigma}_h)_{12}$ (left), and $(\underline{\sigma}_h)_{22}$ (right). Third row: Plot of the discrete approximate energies E_h (blue straight line) and $\tilde{E}_h$ (red oscillatory line) defined in (19) and (20), respectively.

and initial conditions

$$\boldsymbol{u}(x, y, t = 0) = \mathbf{0}, \quad \boldsymbol{v}(x, y, t = 0) = \begin{pmatrix} 0 \\ x \end{pmatrix}.$$

We compute until final time $T = 10$ and with material parameters Young's modulus $E = 20$, Poisson's ratio $\nu = 1/3$. We take $h = 6.25 \times 10^{-3}$, $\Delta t = 2.853 \times 10^{-4}$, $k = 1$ and $\tau = 1/h$.

In Fig. 4, we plot the approximate solutions $(\boldsymbol{u}_h)_2$, $(\underline{\boldsymbol{\sigma}}_h)_{11}$, $(\underline{\boldsymbol{\sigma}}_h)_{12}$, and $(\underline{\boldsymbol{\sigma}}_h)_{22}$. Finally, in Fig. 4, we plot the evolution of the error in the energy of E_h and of $\tilde{E}_h$ in time. We observe no energy dissipation in time.

7. Extensions

What we have presented here can be extended to many other finite element methods including the continuous Galerkin method, mixed methods arising from the application of the Hu-Washizu variational principle, and to DG and HDG methods presented in non-mixed form like in [22, 28]. It can also be extended to other equations of mathematical physics displaying Hamiltonian structure. The extension to nonlinear elastodynamics and Maxwell's equations constitute the subject of ongoing work.

Acknowledgements. The authors would like to thank J.M. Sanz-Serna for clarifications on the properties of the ESPRK methods used in this paper. They would also thank two anonymous referees for their constructive criticism. In particular, they are grateful for bringing to their attention the references [6, 21] about pioneering work on this subject and the references [5, 9, 25] on finite element methods with Hamiltonian structure.

Appendix A. An auxiliary result

Lemma Appendix A.1. *Let* $\boldsymbol{w} \in \mathbb{R}^d$ *and* $\underline{\boldsymbol{\chi}} \in \mathbb{R}^{d\times d}$. *Then*

$$\langle \boldsymbol{w}, \underline{\boldsymbol{\chi}}\boldsymbol{n}\rangle_{\partial\mathcal{T}_h} = \langle \{\!\{\boldsymbol{w}\}\!\} \cdot [\![\underline{\boldsymbol{\chi}}\boldsymbol{n}]\!] + [\![\boldsymbol{w}\otimes\boldsymbol{n}]\!] : \{\!\{\underline{\boldsymbol{\chi}}\}\!\}, 1\rangle_{\mathcal{F}_h^0} + \langle \boldsymbol{w}, \underline{\boldsymbol{\chi}}\boldsymbol{n}\rangle_{\mathcal{F}_h^D\cup\mathcal{F}_h^N}.$$

Proof. We use the definition of the product $\langle\cdot,\cdot\rangle_{\partial\mathcal{T}_h}$ and decompose it into a sum over the faces in $\mathcal{F}_h$. For an interior face $F \in \mathcal{F}_h^0$, there exist $K_1, K_2 \in \mathcal{T}_h$ with $F = \partial K_1 \cap \partial K_2$. With this notation, we have

$$\begin{aligned}
&\langle \boldsymbol{w}|_{K_1}, \underline{\boldsymbol{\chi}}|_{K_1}\boldsymbol{n}|_{K_1}\rangle_F + \langle \boldsymbol{w}|_{K_2}, \underline{\boldsymbol{\chi}}|_{K_2}\boldsymbol{n}|_{K_2}\rangle_F \\
&= \langle \boldsymbol{w}|_{K_1} + \frac{1}{2}\left(\boldsymbol{w}|_{K_2} - \boldsymbol{w}|_{K_2}\right), \underline{\boldsymbol{\chi}}|_{K_1}\boldsymbol{n}|_{K_1}\rangle_F + \langle \boldsymbol{w}|_{K_2} + \frac{1}{2}\left(\boldsymbol{w}|_{K_1} - \boldsymbol{w}|_{K_1}\right), \underline{\boldsymbol{\chi}}|_{K_2}\boldsymbol{n}|_{K_2}\rangle_F \\
&= \langle \{\!\{\boldsymbol{w}\}\!\}, \underline{\boldsymbol{\chi}}|_{K_1}\boldsymbol{n}|_{K_1} + \underline{\boldsymbol{\chi}}|_{K_2}\boldsymbol{n}|_{K_2}\rangle_F + \langle \frac{1}{2}\left(\boldsymbol{w}|_{K_1} - \boldsymbol{w}|_{K_2}\right), \underline{\boldsymbol{\chi}}|_{K_1}\boldsymbol{n}|_{K_1} - \underline{\boldsymbol{\chi}}|_{K_2}\boldsymbol{n}|_{K_2}\rangle_F \\
&= \langle \{\!\{\boldsymbol{w}\}\!\}, [\![\underline{\boldsymbol{\chi}}\boldsymbol{n}]\!]\rangle_F + \langle \boldsymbol{w}|_{K_1}\otimes\boldsymbol{n}|_{K_1} + \boldsymbol{w}|_{K_2}\otimes\boldsymbol{n}|_{K_2}, \frac{1}{2}\underline{\boldsymbol{\chi}}|_{K_1} + \frac{1}{2}\underline{\boldsymbol{\chi}}|_{K_2}\rangle_F \\
&= \langle \{\!\{\boldsymbol{w}\}\!\}, [\![\underline{\boldsymbol{\chi}}\boldsymbol{n}]\!]\rangle_F + \langle [\![\boldsymbol{w}\otimes\boldsymbol{n}]\!], \{\!\{\underline{\boldsymbol{\chi}}\}\!\}\rangle_F,
\end{aligned}$$

which gives the first term of the identity. The second term is straightforward evaluation on boundary faces $\mathcal{F}_h^D$ and $\mathcal{F}_h^N$. $\square$

Appendix B. Solving the global system for the fully discrete HDG method

Here, we show that the global system of the fully discrete HDG method of Subsection 5.2 has a unique solution and can be easily solved.

To alleviate the notation, we drop the superscript ^{n,i}. We begin by noting that the third equation is satisfied when $\widehat{\boldsymbol{\sigma}}_h \boldsymbol{n} = \boldsymbol{\sigma}_N$ on Γ_N and if, on $\mathcal{F}_h^0$ we have

$$\widehat{\boldsymbol{u}}_h = \widetilde{\boldsymbol{u}}_h - \frac{[\![\underline{\boldsymbol{\sigma}}_h \boldsymbol{n}]\!]}{2\{\!\{\tau\}\!\}}$$

where

$$\widetilde{\boldsymbol{u}}_h := \frac{\tau^+}{2\{\!\{\tau\}\!\}} P_M \boldsymbol{u}_h^+ + \frac{\tau^-}{2\{\!\{\tau\}\!\}} P_M \boldsymbol{u}_h^- \quad \text{and} \quad \{\!\{\tau\}\!\} = \frac{1}{2}(\tau^+ + \tau^-).$$

Then, if we set $\widetilde{\boldsymbol{u}}_h := \boldsymbol{u}_D$ on Γ_D, the remaining two equations of the global system in question read

$$\begin{aligned}(\underline{\boldsymbol{\epsilon}}_h, \underline{\boldsymbol{\chi}})_{\mathcal{T}_h} + \zeta_h(\underline{\boldsymbol{\sigma}}_h, \underline{\boldsymbol{\chi}}) &= -(\boldsymbol{u}_h, \nabla \cdot \underline{\boldsymbol{\chi}})_{\mathcal{T}_h} + \langle \widetilde{\boldsymbol{u}}_h, \underline{\boldsymbol{\chi}} \boldsymbol{n} \rangle_{\mathcal{F}_h^0 \cup \Gamma_D} + \langle \frac{\boldsymbol{\sigma}_N}{\tau}, \underline{\boldsymbol{\chi}} \boldsymbol{n} \rangle_{\Gamma_N}, \\ (\underline{\boldsymbol{\sigma}}_h, \underline{\boldsymbol{\chi}})_{\mathcal{T}_h} &= (\mathcal{C} \underline{\boldsymbol{\epsilon}}_h, \underline{\boldsymbol{\chi}})_{\mathcal{T}_h}.\end{aligned}$$

for all $\underline{\boldsymbol{\chi}} \in \underline{\boldsymbol{V}}_h$, where

$$\zeta_h(\underline{\boldsymbol{\sigma}}_h, \underline{\boldsymbol{\chi}}) := \langle \frac{[\![\underline{\boldsymbol{\sigma}}_h \boldsymbol{n}]\!]}{2\{\!\{\tau\}\!\}}, [\![\underline{\boldsymbol{\chi}} \boldsymbol{n}]\!] \rangle_{\mathcal{F}_h^0} + \langle \frac{\underline{\boldsymbol{\sigma}}_h \boldsymbol{n}}{\tau}, \underline{\boldsymbol{\chi}} \boldsymbol{n} \rangle_{\Gamma_N}.$$

We can now see that the global system is uniquely solvable since the bilinear form ζ_h only adds a non-negative, symmetric matrix to the mass matrix. The global system can be computed at the very beginning of the simulation and can be solved easily at each inner step of the time-marching method. For example, for the HDG$_k$+ used in our numerical experiments, τ is of order $1/h$ and a simple block-Jacobi iteration converges with a number of iterations independent of the mesh.

Appendix C. The ESPRK methods we use

Partitioned RK methods satisfying the condition

$$b_i \tilde{a}_{ij} + \tilde{b}_j a_{ji} - b_i \tilde{b}_j = 0 \qquad \text{for } i, j = 1, \ldots, s,$$

are symplectic when applied to *separable* Hamiltonians, see [1, Theorem 2.1]. The Butcher tableaux associated with the ESPRK schemes we use in our experiments have the structure displayed in Table C.3. So, a simple computation shows that they satisfy the above condition; see also [1, (6.1)]. In other words, they are symplectic when applied to the semidiscrete methods for the elastodynamics equations.

The methods *do* preserve linear invariants, but *not* quadratic invariants like our Hamiltonians. Instead, as they are symplectic, they approximate the Hamiltonian of the corresponding semidiscrete method with *no drift* in time whenever $\boldsymbol{u}_d$, $\boldsymbol{f}$ and $\boldsymbol{\sigma}_N$ are independent of time.

In Table Appendix C, we display the coefficients of the Explicit Symplectic Partitioned Runge-Kutta schemes, of s-stages and p-order, ESPRK(s, p), used in our computations. In the section of numerical experiments, we refer to them simply by ESPRK(p).

$$
\begin{array}{cccc|c}
b_1 & 0 & \dots & 0 & b_1 \\
b_1 & b_2 & \ddots & \vdots & b_1+b_2 \\
\vdots & \vdots & \ddots & 0 & \vdots \\
b_1 & b_2 & \dots & b_s & \displaystyle\sum_{i=1}^{s} b_i \\
\hline
b_1 & b_2 & \dots & b_s &
\end{array}
\qquad
\begin{array}{ccccc|c}
0 & 0 & \dots & & 0 & 0 \\
\tilde{b}_1 & 0 & \ddots & & \vdots & \tilde{b}_1 \\
\tilde{b}_1 & \tilde{b}_2 & \ddots & & & \tilde{b}_1+\tilde{b}_2 \\
\vdots & \vdots & \ddots & 0 & 0 & \vdots \\
\tilde{b}_1 & \tilde{b}_2 & \dots & \tilde{b}_{s-1} & 0 & \displaystyle\sum_{i=1}^{s-1} \tilde{b}_i \\
\hline
\tilde{b}_1 & \tilde{b}_2 & \dots & \tilde{b}_{s-1} & \tilde{b}_s &
\end{array}
$$

Table C.3: Butcher tableaux of s-stages partitioned Runge-Kutta methods

i	b_i	$\tilde{b}_i$
1	$7/24$	$2/3$
2	$3/4$	$-2/3$
3	$-1/24$	1

i	b_i	$\tilde{b}_i$
1	$7/48$	$1/3$
2	$3/8$	$-1/3$
3	$-1/48$	1
4	$-1/48$	$-1/3$
5	$3/8$	$1/3$
6	$7/48$	0

i	b_i	$\tilde{b}_i$
1	0.119390029287567275 8	0.339839625839110000
2	0.6989273703824752308	-0.088601336903027329
3	-0.17131235827160077 54	0.5858564768259621188
4	0.4012695022513534480	-0.6030393565364911888
5	0.0107050818482359840	0.3235807965546976394
6	-0.0589796254980311632	0.4423637942197494587

i	b_i	$\tilde{b}_i$
1	0.0502627644003922	0.148816447901042
2	0.413514300428344	-0.132385865767784
3	0.0450798897943977	0.067307604692185
4	-0.188054853819569	0.432666402578175
5	0.541960678450780	-0.016404589403618
6	-0.725525558508690	-0.016404589403618
7	0.541960678450780	0.432666402578175
8	-0.188054853819569	0.067307604692185
9	0.0450798897943977	-0.132385865767784
10	0.413514300428344	0.148816447901042
11	0.0502627644003922	0

References

[1] L. Abia and J.M. Sanz-Serna. Partitioned Runge-Kutta methods for separable Hamiltonians. Math. Comp., 60(202):617–634, 1993.

[2] S. Adams and B. Cockburn. A mixed finite element method for elasticity in three dimensions. J. Sci. Comput., 25:515–521, 2005.

[3] D. Appelö and T. Hagstrom. A new discontinuous Galerkin formulation for wave equations in second-order form. SIAM J. Numer. Anal., 53:2705–2726, 2015.

[4] D. Appelö and T. Hagstrom. An energy-based discontinuous Galerkin discretization of the elastic wave equation in second-order form. Comput. Methods Appl. Mech. Engrg., 338:362–391, 2018.

[5] F. Armero. Assumed strain finite element methods for conserving temporal integrations in non-linear solid dynamics. Internat. J. Numer. Methods Engrg., 74(12):1795–1847, 2008.

[6] F. Armero and I. Romero. On the formulation of high-frequency dissipative time-stepping algorithms for nonlinear dynamics. Part I: low-order methods for two model problems and nonlinear elastodynamics. Comput. Methods Appl. Mech. Engrg., 190(20-21):2603–2649, 2001.

[7] D.N. Arnold, G. Awanou, and R. Winther. Finite elements for symmetric tensors in three dimensions. Math. Comput., 77:1229–1251, 2008.

[8] D.N. Arnold and R. Winther. Mixed finite elements for elasticity. Numer. Math., 92:401–419, 2002.

[9] P. Betsch, A. Janz, and C. Hesch. A mixed variational framework for the design of energy–momentum schemes inspired by the structure of polyconvex stored energy functions. Comput. Methods Appl. Mech. Engrg., 335:660–696, 2018.

[10] P. Ciarlet. The finite element method for elliptic problems. North-Holland, Armsterdam, 1978.

[11] B. Cockburn. Static condensation, hybridization, and the devising of the HDG methods. In G.R. Barrenechea, F. Brezzi, A. Cagniani, and E.H. Georgoulis, editors, Building Bridges: Connections and Challenges in Modern Approaches to Numerical Partial Differential Equations, volume 114 of Lect. Notes Comput. Sci. Engrg., pages 129–177. Springer Verlag, Berlin, 2016. LMS Durham Symposia funded by the London Mathematical Society. Durham, U.K., on July 8–16, 2014.

[12] B. Cockburn and G. Fu. Devising superconvergent HDG methods with symmetric approximate stresses for linear elasticity by M-decompositions. IMA J. Numer. Anal., 38(2):566–604, 2018.

[13] B. Cockburn, M.A. Sánchez, and C. Xiong. Supercloseness of Primal-Dual Galerkin Approximations for Second Order Elliptic Problems. J. Sci. Comput., 75(1):376–394, 2018.

[14] B. Cockburn, D. Schötzau, and J. Wang. Discontinuous Galerkin methods for incompressible elastic materials. Comput. Methods Appl. Mech. Engrg., 195:3184–3204, 2006. C. Dawson, Ed.

[15] S. Du and F.-J. Sayas. New analytical tools for HDG in elasticity, with applications to elastodynamics. Math. Comp., 89:1745–1782, 2020.

[16] O. Gonzalez. Time Integration and Discrete Hamiltonian Systems. Journal of Nonlinear Science, 6(5):449–467, 1996.

[17] O. Gonzalez. Exact energy and momentum conserving algorithms for general models in nonlinear elasticity. Computer Methods in Applied Mechanics and Engineering, 190(13-14):1763–1783, 2000.

[18] O. Gonzalez and J. C. Simo. On the stability of symplectic and energy-momentum algorithms for non-linear Hamiltonian systems with symmetry. Computer Methods in Applied Mechanics and Engineering, 134(3-4):197–222, 1996.

[19] J. Gopalakrishnan and J. Guzmán. Symmetric nonconforming mixed finite elements for linear elasticity. SIAM J. Numer. Anal., 49(4):1504–1520, 2011.

[20] J. Gopalakrishnan and J. Guzmán. A second elasticity element using the matrix bubble. IMA J. Numer. Anal., 32(1):352–372, 2012.

[21] M. Groß, P. Betsch, and P. Steinmann. Conservation properties of a time FE method. Part IV: Higher order energy and momentum conserving schemes. Internat. J. Numer. Methods Engrg., 63(13):1849–1897, 2005.

[22] P. Hansbo and M.G. Larson. Discontinuous finite element methods for incompressible and nearly incompressible elasticity by use of Nitsche's method. Comput. Methods Appl. Mech. Engrg., 191:1895–1908, 2002.

[23] R.C. Kirby and T.T. Kieu. Symplectic-mixed finite element approximation of linear acoustic wave equations. Numer. Math., 130:257–291, 2015.

[24] S. Krenk. Energy conservation in Newmark based time integration algorithms. Computer Methods in Applied Mechanics and Engineering, 195(44-47):6110–6124, 2006.

[25] M. Lavrenčič and B. Brank. Energy-decaying and momentum-conserving schemes for transient simulations with mixed finite elements. Comput. Methods Appl. Mech. Engrg., 375:113625, 2021.

[26] C. Lehrenfeld. Hybrid discontinuous Galerkin methods for solving incompressible flow problems. PhD thesis, Diplomigenieur Rheinisch-Westfalishen Technischen Hochchule Aachen, 2010.

[27] C. Lehrenfeld and J. Schöberl. High order exactly divergence-free hybrid discontinuous Galerkin methods for unsteady incompressible flows. Comput. Methods Appl. Mech. Engrg., 307:339–361, 2016.

[28] A. Lew, P. Neff, D. Sulsky, and M. Ortiz. Optimal BV estimates for a discontinuous Galerkin method for linear elasticity. AMRX Appl. Math. Res. Express, (3):73–106, 2004.

[29] J.E. Marsden and T.S. Ratiu. Introduction to Mechanics and Symmetry. Springer-Verlag, 1994.

[30] R. McLachlan. Symplectic integration of Hamiltonian wave equations. Numer. Math., 66:465–492, 1994.

[31] N.C. Nguyen and J. Peraire. Hybridizable discontinuous Galerkin methods for Partial differential equations in continuum mechanics. J. Comput. Phys., 231:5955–5988, 2012.

[32] N.C. Nguyen, J. Peraire, and B. Cockburn. High-order implicit hybridizable discontinuous Galerkin methods for acoustics and elastodynamics. J. Comput. Phys., 230:3695–3718, 2011.

[33] S. Nurijanyan, J.J.W. van der Vegt, and O. Bokhove. Hamiltonian discontinuous Galerkin FEM for linear, rotating incompressible Euler equations: Inertial waves. J. Comput. Phys., 241:502–525, 2013.

[34] W. Qiu, J. Shen, and K. Shi. An HDG method for linear elasticity with strong symmetric stresses. Math. Comp., 87(309):69–93, 2018.

[35] W. Qiu, J. Shen, and K. Shi. An HDG method for linear elasticity with strong symmetric stresses. Math. Comp., 87:69–93, 2018.

[36] M.A. Sánchez, C. Ciuca, N.C. Nguyen, J. Peraire, and B. Cockburn. Symplectic Hamiltonian HDG methods for wave propagation phenomena. J. Comput. Phys., 350:951–973, 2017.

[37] J. C. Simo and N. Tarnow. The discrete energy-momentum method. Conserving algorithms for nonlinear elastodynamics. ZAMP Zeitschrift für angewandte Mathematik und Physik, 43(5):757–792, 1992.

[38] J. C. Simo, N. Tarnow, and M. Doblare. Non-linear dynamics of three-dimensional rods: Exact energy and momentum conserving algorithms. Internat. J. Numer. Methods Engrg., 38(9):1431–1473, 1995.

[39] J. C. Simo, N. Tarnow, and K. K. Wong. Exact energy-momentum conserving algorithms and symplectic schemes for nonlinear dynamics. Computer Methods in Applied Mechanics and Engineering, 100(1):63–116, 1992.

[40] S.-C. Soon. Hybridizable discontinuous Galerkin methods for solid mechanics. PhD thesis, University of Minnesota, Minneapolis, 2008.

[41] S.-C. Soon, B. Cockburn, and H.K. Stolarski. A hybridizable discontinuous Galerkin method for linear elasticity. Internat. J. Numer. Methods Engrg., 80(8):1058–1092, 2009.

[42] Y. Xu, J.J.W. van der Vegt, and O. Bokhove. Discontinuous Hamiltonian finite element method for linear hyperbolic systems. J. Sci. Comput., 35:241–265, 2008.

[43] J Yan and C.-W. Shu. Local discontinuous Galerkin methods for Partial differential equations with higher order derivatives. J. Sci. Comput., 17:27–47, 2002.